



ELSEVIER

Journal of Volcanology and Geothermal Research 110 (2001) 235–263

www.elsevier.com/locate/jvolgeores

Journal of volcanology
and geothermal research

Magma dynamics, crystallization, and chemical differentiation of the 1959 Kilauea Iki lava lake, Hawaii, revisited

A. Mark Jellinek^{a,*}, Ross C. Kerr^b

^a*Department of Earth and Planetary Science, University of California at Berkeley, 307 McCone Hall, Berkeley, CA 94720, USA*

^b*Research School of Earth Sciences, Australian National University, Canberra ACT 0200, Australia*

Abstract

Using constraints from an extensive database of geological and geochemical observations along with results from fluid mechanical studies of convection in magma chambers, we identify the main physical processes at work during the solidification of the 1959 Kilauea Iki lava lake. In turn, we investigate their quantitative influence on the crystallization and chemical differentiation of the magma, and on the development of the internal structure of the lava lake. In contrast to previous studies, vigorous stirring in the magma, driven predominately by the descent of dense crystal-laden thermal plumes from the roof solidification front and the ascent of buoyant compositional plumes due to the in situ growth of olivine crystals at the floor, is predicted to have been an inevitable consequence of very strong cooling at the roof and floor. The flow is expected to have caused extensive but imperfect mixing over most of the cooling history of the magma, producing minor compositional stratification at the roof and thermal stratification at the floor. The efficient stirring of the large roof cooling is expected to have resulted in significant internal nucleation of olivine crystals, which ultimately settled to the floor. Additional forcing due to either crystal sedimentation or the ascent of gas bubbles is not expected to have increased significantly the amount of mixing. In addition to convection in the magma, circulation driven by the convection of buoyant interstitial melt in highly permeable crystal-melt mushes forming the roof and the floor of the lava lake is envisaged to have produced a net upward flow of evolved magma from the floor during solidification. In the floor zone, mush convection may have caused the formation of axisymmetric chimneys through which evolved magma drained from deep within the floor into the overlying magma and potentially the roof. We hypothesize that the highly evolved, pipe-like ‘vertical olivine-rich bodies’ (VORBs) [Helz, 1980 *Bull. Volcanol.* 43 (1980) 675] observed in the floor zone of the lake are fossil chimneys. In the roof zone, buoyant residual liquid both produced at the roof solidification front and gained from the floor as a result of incomplete convective mixing is envisaged to have percolated or ‘leaked’ into the overlying highly-permeable cumulate, displacing less buoyant interstitial melt downward. The results from Rayleigh fractionation-type models formulated using boundary conditions based on a quantitative understanding of the convection in the magma indicate that most of the incompatible element variation over the height of the lake can be explained as a consequence of a combination of crystal settling and the extensive but imperfect convective mixing of buoyant residual liquid released from the floor solidification front. The remaining chemical variation is understood in terms of the additional influences of mush convection in the roof and floor on the vertical distribution of incompatible elements. Although cooling was concentrated at the roof of the lake, the floor zone is found to be thicker than the roof zone, implying that it grew more quickly. The large growth rate of the floor is explained as a consequence of a combination of the substantial sedimentation of olivine crystals and more rapid in situ crystallization due to both a higher liquidus temperature and enhanced cooling resulting from imperfect thermal and chemical mixing. © 2001 Elsevier Science B.V. All rights reserved.

Keywords: magma dynamics; crystallization; Kilauea Iki lava lake

* Corresponding author. Tel.: +1-510-642-6331; fax: +1-510-643-9980.

E-mail addresses: markj@seismo.berkeley.edu (A.M. Jellinek), ross.kerr@anu.edu.au (R.C. Kerr).

1. Introduction

Over the last two decades, the results from a large number of fluid dynamical studies have shown that convective motions play an important part in the solidification and differentiation of basaltic magma chambers (Turner and Campbell, 1986; Martin et al., 1987; Jaupart and Tait, 1995; Jellinek et al., 1999; Jellinek and Kerr, 1999). For some time, the qualitative application of well-understood principles of convection in magma chambers has led to large breakthroughs in the understanding of geological data sets (e.g. McBirney and Noyes, 1979; McBirney, 1995; Campbell, 1996). However, the quantitative application of the results of fluid dynamical studies to the understanding of particular igneous bodies has

been generally inhibited by limitations imposed by the complex nature of many geological and geochemical data sets. In contrast to many well-studied magma chambers, the results from a program of continuous monitoring and drilling of the 1959 Kilauea Iki lava lake (Fig. 1) have led to good constraints on the geometry and internal structure of the lava lake as well as the cooling, physical properties, and compositional evolution of the magma. Accordingly, the goals of this study are first to use geological data to identify and understand the main physical processes at work during the solidification of the lava lake, and then to investigate how these processes influenced quantitatively the solidification and chemical differentiation of the magma.

A significant result of our analysis is that strong

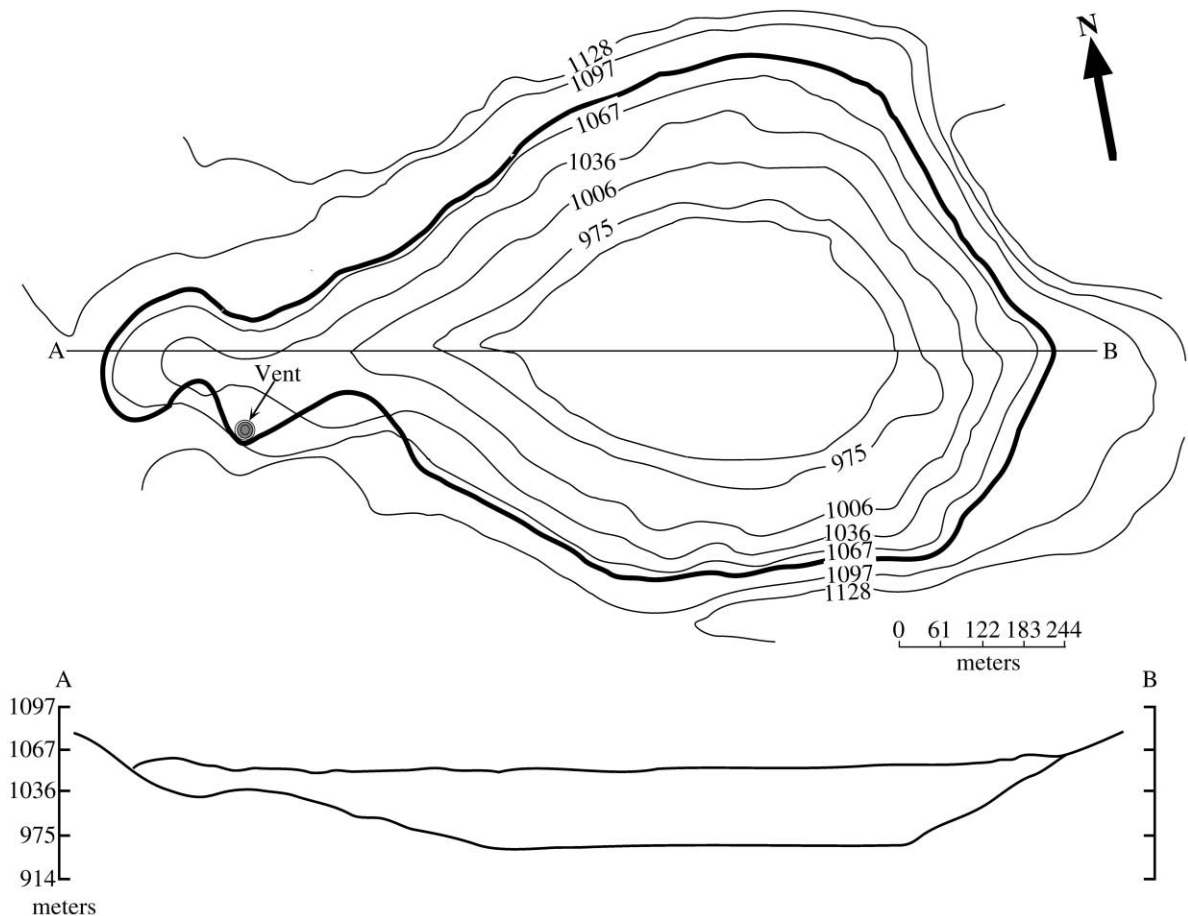


Fig. 1. Map and cross section of the 1959 Kilauea Iki lava lake reproduced from the study by Richter and Moore (1966).

cooling at the roof and floor of the lake led inevitably to thermal, compositional, and particle (bubbles and crystals) buoyancy sources during solidification of the lake, which drove chaotic, time-dependent (or vigorous) motions that stirred the magma, producing extensive thermal and chemical mixing over most of the solidification history of the lava lake. This very dynamic picture is in marked contrast with the view of Helz (1980) that lava-lake convection ‘either did not occur at all or was active only briefly’ (and with the view of Helz et al. (1989a) that diapiric transfer of melt from the floor, through the overlying magma, and into the roof occurred ‘without mixing’), but is consistent with the arguments for convection in Kilauea lava lakes given by Wright et al. (1976). Our work is also in marked contrast with a number of studies (e.g. Marsh, 1988) in which convection in magma chambers is taken to be absent or weak (and ‘never vigorous’) — an assertion that has been shown to be fluid-mechanically incorrect in most basaltic systems (e.g. Martin et al., 1987; Carrigan, 1987; Worster et al., 1991; Huppert and Turner, 1991; Davaille and Jaupart, 1993b; Worster et al., 1993; Jaupart and Tait, 1995; Jellinek and Kerr, 1999). In addition, the convection of interstitial melt in the growing floor and roof zones may have also been important. To understand the convection in the magma we apply results from an extensive series of experiments designed to quantify mixing by natural convection, which were presented in Jellinek et al. (1999). In the majority of these experiments, a compositionally buoyant (input) fluid was injected at a fixed rate into an overlying (ambient) layer of denser fluid from a planar source. The structure of the resulting convective motions, and hence the amount of mixing, was found to depend on a Reynolds number based on the height of the ambient layer of fluid

$$Re \sim \frac{B^{1/3} H_a^{4/3}}{\nu_a} \quad (1)$$

and the ratio

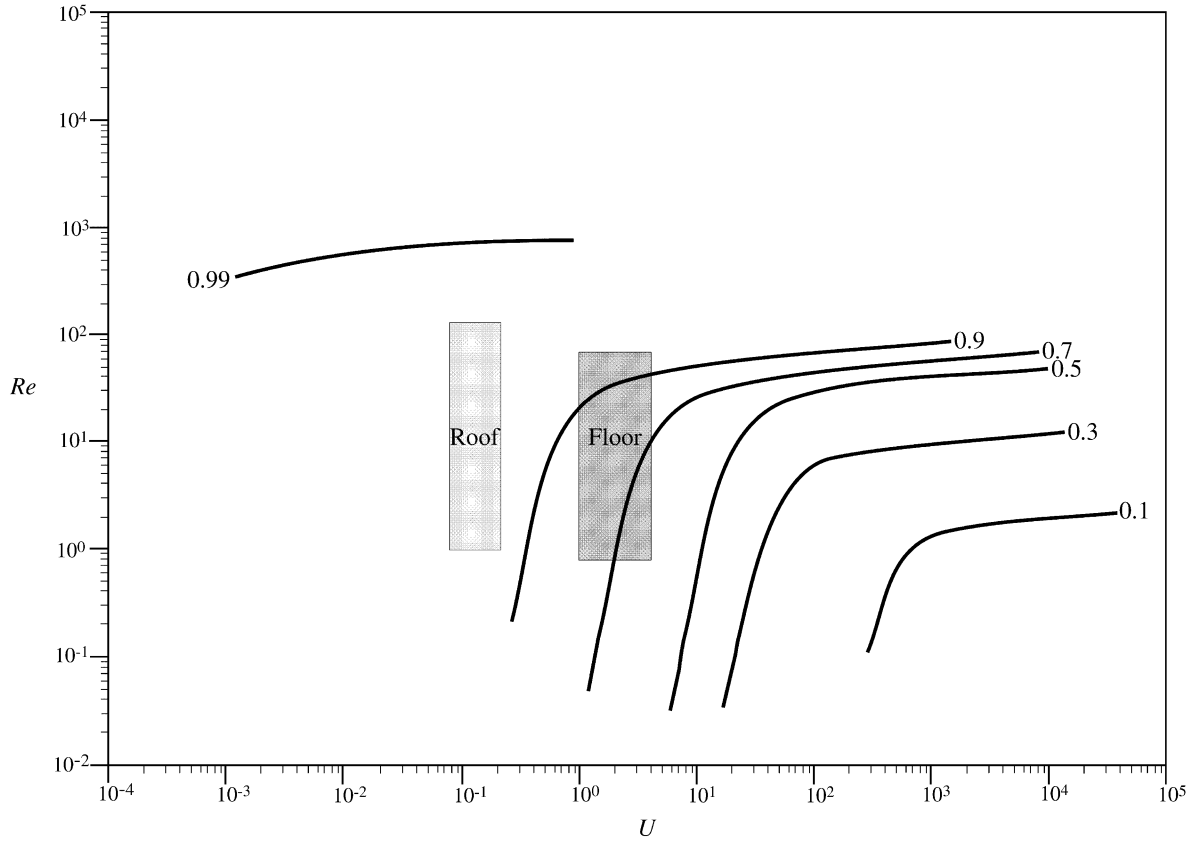
$$U = \frac{\nu_a}{\nu_i} \quad (2)$$

of the ambient fluid kinematic viscosity to the input fluid kinematic viscosity. Here H_a and ν_a are the height and kinematic viscosity of the ambient fluid

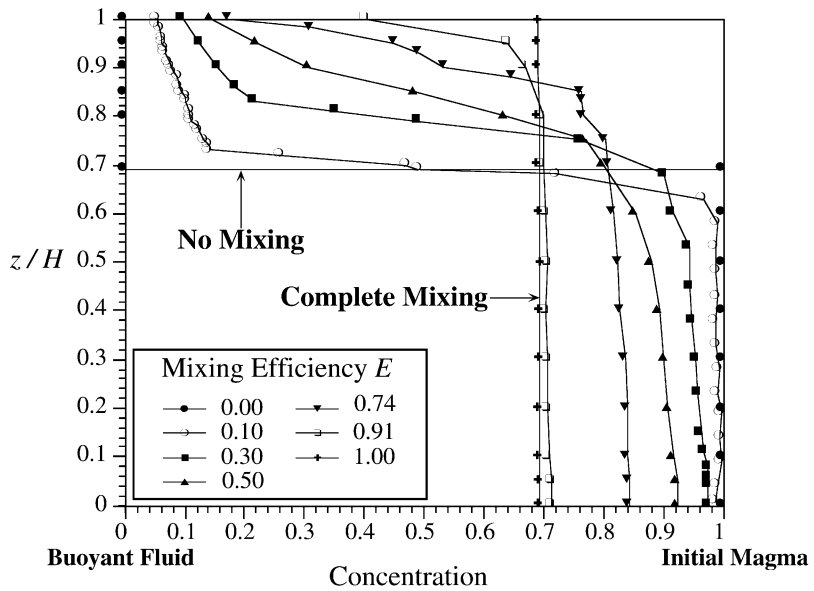
layer; ν_i is the kinematic viscosity of the input fluid, and $B = gV_i[(\rho_a - \rho_i)/\rho_a]$ is the weight deficiency per unit time and area supplied from the boundary (buoyancy flux), where g is the gravitational acceleration, V_i is the flux per unit area of input fluid, ρ_a is the density of the ambient fluid, and ρ_i is the density of the input fluid (we note that the buoyancy flux B becomes a buoyancy force per unit time and area when it is multiplied by the density of the input fluid ρ_i). The symbol ‘ \sim ’ is used to denote ‘of the order of’. The amount of mixing was quantified in terms of a thermodynamic mixing efficiency E such that complete mixing occurs when $E = 1$, and no mixing occurs when $E = 0$ (Fig. 2b). Extensive mixing ($E > 0.9$) occurred when the interaction between unstable rising plumes and the ambient fluid led to strong large-scale circulation, which disrupted and stirred rising buoyant fluid causing mixing. Very incomplete mixing ($E < 0.1$) or ponding of the buoyant fluid occurred only when its interaction with the ambient fluid during its rise produced negligible large-scale convective motions.

The structure of this paper is as follows. We present a set of geological observations in Section 2 that will be used to constrain the cooling, crystallization, and chemical differentiation of the lava lake. In Section 3 we identify thermal, compositional, and particle (crystals and bubbles) buoyancy sources arising as a result of cooling at the roof and floor of the lake and then evaluate the mixing efficiency of the resulting convective motions. To investigate the influence of the convection in the magma on the chemical differentiation of the lava lake, we apply in Section 4 a quantitative understanding of the flow developed in Section 3 to formulate several plausible Rayleigh fractionation-type models for the chemical differentiation of the lake. The results of these models are then compared with an existing chemical data set. Remaining uncertainties about the chemical variation in the lake are discussed in terms of additional important effects of the convection of interstitial melt anticipated to occur in the roof and floor zones. We note that a significant difference to the modeling approaches established in previous ‘parameterized’ geochemical studies (e.g. Langmuir, 1989) is that our models are tied quantitatively to the predominant convection and crystallization processes at work during the solidification of the lake, and hence are

(a)



(b)



developed in an essentially ‘forward’ way. We close Section 4 with a comparison of our analysis of the chemical differentiation of the lake with that done by Helz et al. (1989a). In Section 5 we investigate the influence of convection in the magma on the rates of crystallization at the roof and floor of the lake and discuss the significance of the results in terms of the observed internal structure of the lake. We conclude in Section 6.

2. Geological constraints on solidification and differentiation

One of the most difficult challenges for a geologist studying a particular igneous body is to reconstruct the main physical processes influencing its cooling, crystallization, and chemical differentiation from field and geochemical data. In general, analysis is hampered by the complex, equivocal or controversial nature of many geological data sets. As a result, it is often difficult to constrain the relevant boundary conditions determining the heat and mass transport in the magma during solidification. The 1959 Kilauea Iki lava lake, however, is unique among well-documented magma bodies for both its simple emplacement history and the directness with which it could be studied. Real time observations have revealed that the filling of the roughly 120 m deep, saucer-shaped Kilauea Iki pit crater was a consequence of 17 eruptive phases that took place between 14 November and 20 December 1959 (Richter et al., 1966). Although the flow of lava associated with each successive eruptive phase disaggregated roof crust formed during previous filling events, causing some of it to founder, the roof crust stabilized in the days following the final seventeenth eruptive phase of 20 December 1959, and allowed the bulk of the lava lake to solidify undisturbed as a self-roofed magma chamber (Richter et al., 1966). Studies of temperature measurements

and core recovered from a program of continuous drilling through the roof of the small magma chamber between 1960 and 1981 have yielded useful controls on the cooling, structure, mineralogy, bulk composition, and volatile content of the lake magma during its solidification (Ault et al., 1961; Richter and Moore, 1966; Helz, 1980, 1987a,b; Helz et al., 1989a,b). We use the following geological constraints obtained from this extensive database of observations to develop an understanding of the cooling, crystallization, and concomitant chemical evolution of the lava lake magma:

(1) The 1959 Kilauea Iki lava lake was a roughly elliptical saucer-shaped body with the approximate dimensions of $600 \times 800 \times 120$ m deep (Richter and Moore, 1966). The sidewalls slope $15\text{--}30^\circ$ (Fig. 1), and the mean depth is around 100 m.

(2) The magma, a weighted mixture of lavas erupted from each of the seventeen eruptive phases, was an olivine-rich basalt emplaced with an average temperature of around 1185°C (Ault et al., 1961). On the basis of analyses of samples from the most voluminous first phase of the eruption (Murata and Richter, 1966; Richter and Murata, 1966), the initial melt contained about 8.47 wt% MgO and 10–15 vol%, 1–8 mm subhedral to rounded, olivine phenocrysts. Using the method of Bottinga and Weill (1970) with partial molar volumes from Nelson and Carmichael (1979) we predicted the density of the melt phase ρ_b to be about 2700 kg m^{-3} . The dynamic viscosity of the magma μ_b , which we define to be predominately a mixture of melt and crystals, is taken to be in the range of 50–200 Pa s (Shaw, 1969), implying a kinematic viscosity $\nu_b = \mu_b/\rho_b$ of $0.02\text{--}0.08 \text{ m}^2 \text{ s}^{-1}$. For these magma properties, an average lava lake depth $H = 100$ m, a minimum phenocryst size of $d_s = 1$ mm, and an olivine crystal density $\rho_{xl} = 3220 \text{ kg m}^{-3}$, a maximum time scale for the sedimentation of this initial population of olivine phenocrysts, which given by the ratio of the lake depth divided by the sedimentation velocity $\tau_s =$

Fig. 2. (a) A contour map illustrating how the mixing efficiency E varies over a large region of Reynolds number Re –viscosity ratio U parameter space. The box labeled ‘roof’ corresponds to the thermal convection expected from the roof of the lava lake. The box labeled ‘floor’ corresponds to the compositional convection anticipated from the floor of the lake. (b) The mixing efficiency expressed in terms of normalized concentration profiles measured at the ends of certain experiments reported in Jellinek et al. (1999). The efficiency E is reflected in both the shapes of the profiles and by the minimum and maximum concentrations reported. Also shown are the theoretical concentration profiles corresponding to no and complete mixing.

$18\mu_b H/g(\rho_{xl} - \rho_b)d_s^2$ (cf. Martin and Nokes, 1988, 1989), is about a year. Hence, most of the crystals observed in the drill cores were produced as a result of post-emplacment crystallization of the lake magma.

(3) During drilling, the position of the 1065°C isotherm was tracked as a function of time (Richter and Moore, 1966; Helz, 1980; Hardee, 1980). This isotherm corresponded to the temperature at which the roof crystal mush had sufficient strength to withstand drilling. Downhole temperature measurements made during each episode of drilling between 1960 and 1976 show that over the first six years of cooling, the depth of the 1065°C isotherm increased at a rate proportional to the square root of time, which is consistent with heat loss by pure conduction (Wright et al., 1976; Hardee, 1980). However, over the next ten years or so, this isotherm descended at an approximately constant rate of around 2.1 m yr⁻¹ (Hardee, 1980; Helz, 1980), implying that the roof heat flux became constant. This transition to a constant roof growth rate has been interpreted to reflect (and analyzed in terms of) enhanced cooling caused by the boiling of rainwater that progressively penetrated into the roof crust (Richter and Moore, 1966; Hardee, 1980). As the local annual rainfall is very high (3.5–4 m) and a flux of steam from the roof crust was observed throughout the solidification history of the lava lake, this interpretation appears plausible. Probable support for the deep penetration of rainwater into the roof crust and the circulation of water and steam is the shape of temperature profiles measured over the top 40 m or so of the lake during drilling in 1975 and 1976 (see Hardee (1980), Fig. 1). In most of these profiles, a constant temperature of about 100°C was obtained over the first 30–35 m of core depth (measured from the top), followed by a nearly linear increase in temperature to about 1000°C over a vertical distance of around 5 m. Hardee (1980) has argued that the constant temperature over most of the thickness of the crust was maintained by a circulation of rainwater and steam driven by the conductive heat flux corresponding to the underlying steep temperature gradient. Indeed, the constant temperature of 100°C may have been fixed by the boiling temperature of H₂O at near atmospheric pressures. Taking the temperature difference (ΔT between the magma and the convectively cooled roof crust to be 900°C,

the thermal conductivity of the roof crust to be 1.6 W m⁻¹ °C⁻¹ (Hardee, 1980), and the conductive length scale l to be 5 m, a heat flux corresponding to the observed temperature gradient is about 300 W m⁻².

(4) Time-dependent temperature profiles were not determined in the same detail at the floor or sidewalls of the lake. However, older basaltic rocks forming the walls and floor of the Kilauea Iki pit crater are highly permeable, both vertically and laterally, and are known to support vigorous ground water flow driven by the large recharge due to the 3.5–4 m annual rainfall at the summit of Kilauea Volcano (e.g. Jackson and Kauahikaua, 1990; Thomas et al., 1990). Heat transfer from the magma particularly to the sloping sidewalls of the lake is envisaged, therefore, to heat water contained within fractures therein and, in turn, drive convective circulation. This additional cooling due to the circulation of ground water may have been augmented by fluid flow related to the well-established hydrothermal system at the summit of Kilauea volcano. Therefore, as at the roof of the lake magma, it is reasonable to assume that the conductive heat flux to the floor and sidewall boundaries was augmented by the circulation and boiling of ground water and hydrothermal fluids. As a result, the heat flux to the sidewalls and floor was likely to be significant, and we take a plausible estimate to be around 100 W m⁻². Significant floor cooling is not unique to the 1959 Kilauea Iki lava lake. In the similar-sized prehistoric Makaopuhi lava lake Moore and Evans (1967) have documented that columnar joints grew from the top and bottom of the lake, meeting just below the middle, indicating that the cooling at the floor of the lake was comparable to the cooling at the roof.

(5) Petrographical analyses of samples taken from drill cores indicate that whereas 1–8 mm subhedral to round olivine phenocrysts constitute 20–30 vol% of the mode over the top 40 m of the lake, at 40 m depth in the core there is a sharp increase in olivine crystallinity to 40–45 vol%, which is nearly constant over the remaining depth in the lake (Helz, 1980). The rock below 40 m has been described by Helz (1980) as a ‘diffuse [olivine] cumulate’ (see also Helz, 1987b). On the basis of these petrographic observations, we take the final cumulate porosity averaged over the full depth of the lake magma to be 50–60 vol%. In

addition to being supported by field observations, we note that this estimate is probably close to the maximum possible initial porosity of a self-supporting cumulate of subhedral to rounded olivine crystals and, hence, is also a good indicator of the initial porosity of the floor. Significantly, this estimated porosity implies also that compaction of the floor (cf. Shirley, 1987; Philpotts et al., 1996) was unlikely to have been very important. The remaining modal volume in a given sample is composed mostly of glass, groundmass clinopyroxene and plagioclase, and vesicles. We note also that cumulus olivine crystals in the lower half of the roof are locally rimmed with pyroxene (Helz, 1987b).

(6) Concentrations of K_2O , TiO_2 and MgO normalized to a suitable average bulk composition for the lake are shown as a function of height in the lake in Fig. 3. Two observations are of particular note. The first is that we do not show data below about 90 m depth in the lake, because of the presence of foundered roof crust in drill core (this foundered roof crust augmented the growth of the floor zone as well as potentially the cooling of the lower part of the lake). Second, the variation K_2O and TiO_2 with height are similar and roughly the mirror image of the variation in MgO concentration with height. This symmetry supports the conclusion of many previous workers that olivine fractionation controlled most of the chemical differentiation of the lake magma (e.g. Richter and Moore, 1966; Helz, 1987a; Helz et al., 1989a). One of the most interesting features in the chemical data shown in Fig. 3 is the sharp reversal in trends for both incompatible and compatible elements at about 40 m. The nearly exact correspondence between these reversals and the position at which there is a large increase in olivine crystallinity is very striking, and we take it to record the point in the solidification history of the lava lake at which the growing floor zone met the growing roof zone. There are two significant implications for the boundary between the roof and the floor (a nominal ‘sandwich horizon’) occurring at 40 m depth in the lake that will be useful to our modeling. First, this conclusion implies that although cooling was predominately at the roof, the floor zone grew more quickly. Second, because drilling could penetrate to 44 m in 1975 a maximum estimate for the time required for the floor to meet the roof is 15 yr. We note, however,

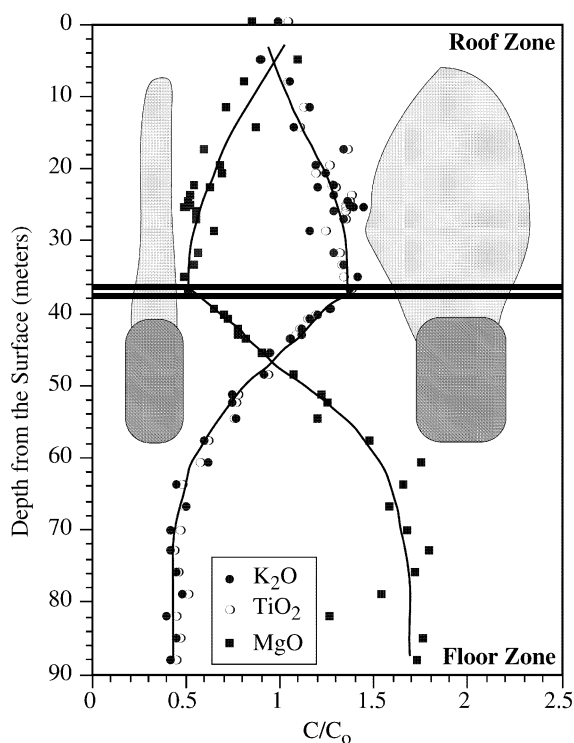


Fig. 3. Plot showing the symmetrical variation of compatible (MgO) and incompatible (TiO_2 and K_2O) components. Also shown are the fields for segregation veins (light gray shading) and for the interstitial melt in VORBs (dark gray shading), which are both depleted in MgO and enriched in TiO_2 and K_2O . The inferred boundary between the roof and floor zones is shown as a heavy double line. The chemical data are from Helz et al. (1989b) and have been normalized using an average bulk composition obtained from analyses of samples of pumice and spatter from the most voluminous phase 1 eruption reported in Murata and Richter (1966).

that the floor probably met the roof well before 1975, because the maximum temperature for drilling ($1065^{\circ}C$) corresponds to significantly more crystallization than the 40–50% crystallinity of the floor mush.

(7) In addition to the roof and floor olivine cumulates and the chemical variation shown in Fig. 3, the effects of physical processes significant to the differentiation of the lava lake are recorded by ‘segregation veins’ and ‘vertical olivine-rich bodies’ (VORBs) (Richter and Moore, 1966; Helz, 1980). Segregation veins are large-aspect-ratio ($\geq 100:1$), roughly horizontal bodies that are 0.1–1 m thick. The veins are highly differentiated, with a molecular $MgO/(MgO +$

FeO) of about 41 (as opposed to a value of 76 more typical for the host basalt) that corresponds to about 50% olivine crystallization. The veins have been observed in core taken as early as 1962, and it appears that the ‘formation and emplacement of segregation veins has been a regularly recurring, major process of

internal differentiation within Kilauea Iki’ (Helz, 1980). Segregation veins are observed predominately in drill cores taken from the center of the lava lake and are located mostly in the roof zone, of which they comprise as much as 10 vol%. Petrographically, they are aphyric and olivine poor with groundmass

Table 1

Parameters used in physical modeling (Most of the physical properties listed were obtained from Shaw (1969), Hardee (1980), Huppert and Sparks (1988), and Chakraborty (1995). The fractionation density of forsterite was estimated from Sparks and Huppert (1984))

Parameter	Symbol	Value and/or unit
Thermal buoyancy flux	B_t	$\text{m}^2 \text{s}^{-3}$
Latent heat buoyancy flux	B_L	$\text{m}^2 \text{s}^{-3}$
Buoyancy flux from a crystal-rich thermal boundary layer	B_t^c	$\text{m}^2 \text{s}^{-3}$
Compositional buoyancy flux	B_c	$\text{m}^2 \text{s}^{-3}$
Specific heat of the basalt	c_b	$1340 \text{ J kg}^{-1} \text{ }^\circ\text{C}^{-1}$
Effective specific heat	c_e	$\text{J kg}^{-1} \text{ }^\circ\text{C}^{-1}$
Crystal diameter	d_s	Mm
Chimney diameter	d	M
Slope of liquidus in T – S space	$\frac{\partial T}{\partial S}$	$7 \times 10^2 \text{ }^\circ\text{C}$
Mixing efficiency	E	–
Height of the lava lake	H	M
Latent heat	L	$8.4 \times 10^5 \text{ J kg}^{-1}$
Gravitational acceleration	g	9.8 m s^{-2}
Critical floor height for mush convection	h_f^c	M
Roof heat flux	q_r	300 W m^{-2}
Floor heat flux	q_f	$100\text{--}150 \text{ W m}^{-2}$
Flow rate	Q	$\text{m}^3 \text{ s}^{-1}$
Reynolds number	Re	–
Temperature	T	$^\circ\text{C}$
Temperature difference	ΔT	$^\circ\text{C}$
Viscosity ratio	U	–
Stokes velocity	V_s	m s^{-1}
Solidification rate	V_c	m s^{-1}
Volume fraction of crystals	X	–
Thermal expansion coefficient of the basalt	α	$5 \times 10^{-5} \text{ }^\circ\text{C}^{-1}$
Effective thermal expansion coefficient	α_e	$^\circ\text{C}^{-1}$
Thermal boundary layer thickness	δ_t	M
Thermal diffusivity of the basalt	κ_t	$10^{-6} \text{ m}^2 \text{ s}^{-1}$
Thermal diffusivity of the floor mush	κ_m	$10^{-6} \text{ m}^2 \text{ s}^{-1}$
Compositional diffusivity	κ_s	$10^{-12} \text{ m}^2 \text{ s}^{-1}$
Dynamic viscosity of the magma	μ_b	$50\text{--}200 \text{ Pa s}$
Kinematic viscosity of the magma	ν_b	$0.02\text{--}0.08 \text{ m}^2 \text{ s}^{-1}$
Kinematic viscosity of interstitial melt	ν_m	$0.05 \text{ m}^2 \text{ s}^{-1}$
Average permeability of the roof and floor ^a	χ	$1.1 \times 10^{-7} \text{ m}^{-2}$
Density of the melt	ρ_b	2700 kg m^{-3}
Density of olivine crystal	ρ_{xl}	3220 kg m^{-3}
Density difference between olivine and magma	$\Delta\rho_{xl}$	520 kg m^{-3}
Fractionation density of olivine	ρ_{fr}	2950 kg m^{-3}
Density difference across the compositional boundary layer	$\Delta\rho_c$	250 kg m^{-3}
Density of interstitial melt	ρ_m	kg m^{-3}
Density difference driving mush convection	$\Delta\rho_m$	300 kg m^{-3}

^a Calculated using the Kozeny–Carman equation and a mean crystal diameter of 2 mm.

crystallinities dominated by plagioclase and augite. VORBs are ‘irregular pipe-like bodies, found principally between 40 and 58 m below the lake surface, [which] extend vertically up the side of the core, and are locally traceable for a meter or more’ (Helz, 1987a). In addition, these bodies are at least centimeters in diameter and probably more than 10 cm apart (two VORBs were never observed in the same sample of drill core). VORBs have interstitial compositions similar to segregation veins, are enriched in relatively coarse (≤ 1 cm as opposed to ≤ 1 mm), iron-rich olivine (F_{077-79} as opposed to more typical F_{086-87}), and have significantly greater versicle concentrations than adjacent host rock (Helz, 1980). Segregation veins and VORBs are observed also in cliff exposures of the prehistoric Makaopuhi lava lake (Moore and Evans, 1967), where, like Kilauea Iki, the segregation veins are confined largely to the roof (the upper tier of columnar joints) and VORBs are restricted mostly to the floor (the lower tier of columnar joints).

3. Potential sources of buoyancy

3.1. Buoyancy fluxes due to cooling at the roof

Rapid cooling at the roof is predicted to cause a boundary layer of thermally dense magma to grow in thickness. Where this layer becomes sufficiently thick it will detach from the roof and descend into the underlying magma as a thermal plume. Over time, the intermittent release and descent of thermal plumes from the roof is envisaged to generate motions in the magma, which in turn, may cause the magma to cool in a nearly uniform way (e.g. Martin et al., 1987; Carrigan, 1987; Kerr et al., 1989). A buoyancy flux due to the release of thermal boundary layer fluid caused by the roof heat flux q_r is given by

$$B_t \sim \frac{q_r \alpha g}{\rho_b c_b}, \quad (3)$$

where α , ρ_b , and c_b are the thermal expansion coefficient, density and specific heat of the magma, and g is the gravitational acceleration. For the parameters given in Table 1, this buoyancy flux is of order $4.1 \times 10^{-8} \text{ m}^2 \text{ s}^{-3}$. We note that to obtain a buoyancy force per area and time this buoyancy flux

can be multiplied by the density of the magma ρ_b to give $1.1 \times 10^{-4} \text{ N m}^{-2} \text{ s}^{-1}$.

When compared with tall crustal magma chambers, which are cooled by heat fluxes of about $0.4\text{--}4 \text{ W m}^{-2}$ (Martin et al., 1987), the roof heat flux $q \approx 300 \text{ W m}^{-2}$ is very large. A significant consequence of this large cooling rate is that the temperature gradient through the thermal boundary layer will be very steep, producing potentially a supersaturation sufficient both to augment existing cumulus crystals and to nucleate new crystals in boundary layer fluid ahead of the solidification front (Martin, 1990). Whether suspended crystals of olivine will augment the buoyancy of the thermal boundary layer, or settle into the underlying magma as an independent source of buoyancy, depends principally on whether the sedimentation rate of the crystals is greater than the growth rate of the roof thermal boundary layer (Sparks et al., 1993; Jarvis and Woods, 1994). Balancing the Stokes settling velocity for roughly spherical olivine crystals

$$V_s = \frac{\Delta\rho_{xl} g d_s^2}{18\rho_b \nu_b} \quad (4)$$

with the diffusive growth velocity of the thermal boundary layer

$$V_t \sim \frac{\kappa_t}{\delta_t}, \quad (5)$$

where

$$\delta_t \sim 10 \left(\frac{\nu_b \kappa_t}{g \alpha \Delta T} \right)^{1/3} \quad (6)$$

(Turner, 1973, p. 227) leads to crystal diameter

$$d_s \sim \left[\frac{1.8\rho_b}{\Delta\rho_{xl}} (\alpha \Delta T)^{1/3} \left(\frac{\nu_b \kappa_t}{g} \right)^{2/3} \right]^{1/2} \quad (7)$$

at which the two rates are approximately equal. Here $\Delta\rho_{xl}$ is the density difference between olivine crystals and the surrounding magma, κ_t is the thermal diffusivity of the magma, and ΔT is the temperature difference driving thermal convection. The choice for ΔT requires some discussion. As the viscosity of magmas increases strongly with cooling and crystal content the large temperature difference from the magma, across the thermal boundary layer, to the cold roof crust implies a steep gradient in viscosity that is potentially augmented by a similar gradient in

crystal concentration and possibly gas bubbles. The experiments and scaling theory of Davaille and Jaupart (1993a) have shown that a significant effect of a steep gradient in viscosity is to stabilize most of the thickness of the thermal boundary layer to gravitational instabilities that would otherwise cause it to drain. For Kilauea Iki, the part of the thermal boundary layer involved actively in driving convection will be a thickness corresponding to a viscosity difference to the underlying magma of about one order of magnitude, implying a temperature difference ΔT of 60–80°C (cf. Davaille and Jaupart, 1993b). Substitution of the relevant parameters from Table 1 and a ΔT of 70°C into Eqs. (5) and (6) leads to a critical thermal boundary layer thickness of about 80 mm and a diameter d_s of 2–4 mm, which is comparable to the sizes of cumulus olivine crystals in the roof and floor zones. Therefore, whereas crystals with a diameter smaller than 2–4 mm will augment the buoyancy of the thermal boundary layer, crystals larger than 2–4 mm will settle into the underlying magma prior to the onset of the gravitational instability causing the boundary layer to detach. However, the time scale to grow a 2–4 mm crystal of olivine by diffusion d_s^2/κ_s , where κ_s is a compositional diffusivity, is 2–6 months while the time scale for the gravitational instability δ_l^2/κ_l of the thermal boundary layer is a few hours. Hence, we can conclude that rather than settling, most crystals nucleated within the thermal boundary layer will remain there, thereby increasing its mean density and buoyancy. We note, however, that after the boundary layer detaches and descends, entrained crystals will become dispersed by the convective motions and ultimately settle to the floor (Martin and Nokes, 1988, 1989).

The release of latent heat and the volume change associated with the growth of olivine crystals will alter the mean heat capacity and thermal expansion coefficient of the thermal boundary layer magma. The magnitude of these effects depends on the crystal content in the thermal boundary layer, which in turn, depends on the imposed temperature gradient. As olivine was initially the only liquidus phase and persisted as the only cumulus phase over the course of solidification, we can use an initial temperature $T = 1185^\circ\text{C}$ with the Roeder and Emslie (1970) relationship between Fe/Mg ratios in olivine and coexisting

melt and the MgO thermometer of Helz and Thornber (1987) to obtain rough estimates of the crystal content as a function of temperature in the boundary layer. Over the temperature range 1185–1110°C (which corresponds to about 0–50% olivine crystallization after the filling of the lake), an empirical expression for the olivine crystal fraction X as an approximate function of temperature T is

$$X = 5.0698 \times 10^{-5} T^2 - 0.1232 T + 74.8429, \quad (8)$$

which can be used in expressions for the effective heat capacity

$$c_e = c_b - L \frac{dX}{dT} \quad (9)$$

and the effective coefficient of thermal expansion of the thermal boundary layer magma

$$\alpha_e = \alpha - \frac{\rho_{xl} - \rho_{fr}}{\rho_b} \frac{dX}{dT} \quad (10)$$

(Kerr, 1994). Here, L is the latent heat of crystallization of olivine and $\rho_{fr} = 2950 \text{ kg m}^{-3}$ is the fractionation density (defined by Sparks and Huppert (1984) as the bulk density of the components selectively extracted from the melt to grow crystals) of olivine with a composition of around Fo_{85} . Taking the temperature difference across the unstable part of the boundary layer to be 70°C and the temperature of the magma to be about 1185°C, the mean boundary layer temperature is 1150°C, implying through Eq. (8) a crystal content of about 21 vol%. Applying Eq. (8) and values from Table 1 to Eqs. (9) and (10), we obtain an effective thermal expansion coefficient $\alpha_e = 8.3 \times 10^{-4} \text{ }^\circ\text{C}^{-1}$ and an effective specific heat $c_e = 6.9 \times 10^3 \text{ J kg}^{-1}$. Substituting these values for α and c_b in Eq. (3) gives an effective thermal buoyancy flux per area $B_l^e = 1.3 \times 10^{-7} \text{ m}^2 \text{ s}^{-3}$ (or alternatively $3.6 \times 10^{-4} \text{ N m}^{-2} \text{ s}^{-1}$), which is about three times larger than the buoyancy flux obtained with Eq. (3).

An additional consequence of very strong cooling at the roof is that the stirring associated with large-scale convective motions will probably cause a significant supersaturation of the whole layer of magma and, in turn, the internal nucleation and growth of olivine crystals (Kerr et al., 1989, 1990; Martin, 1990; Worster et al., 1993; Hort, 1997). From the margins of these crystals, buoyant residual liquid will be produced (see experiments by

Seedhouse and Donaldson, 1996). Since the compositional boundary layers adjacent to crystal-liquid interfaces will be very thin, we expect that this residual liquid will be entrained into the magma and extensively mixed (cf. Kerr, 1995; Jellinek et al., 1999). In addition, the ultimate sedimentation of crystals nucleated internally will augment the growth of the floor.

Reynolds numbers (see Eq. (1)) based on B_t and B_t^c are shown as a function of height in Fig. 4 for kinematic viscosities ν_b of 0.02 and 0.08 m² s⁻¹. For an initial lake depth $H = 100$ m, Reynolds numbers for the convection driven by the descent of crystal free thermal plumes are around 85 and 20, respectively. With the additional buoyancy in the thermal boundary layer due to 21 vol% crystals, these Reynolds numbers increase to 118 and 28, respectively. In contrast, when the lake depth is $H = 10$ m, Reynolds numbers based on B_t are about 3.4 and 1, while Reynolds numbers based on B_t^c are 5.5 and 1.3. For the case of no crystals the viscosity ratio U averaged across the unstable part of the thermal boundary layer is about 0.2. The addition of 21 vol% crystals will increase the average viscosity of the thermal boundary layer by about a factor of 2.5 (cf. Roscoe, 1953) which, in turn, reduces the viscosity ratio U to about 0.08. In Fig. 2a we have drawn a shaded box indicating the Reynolds number Re -viscosity ratio U parameter space corresponding to the thermal convection anticipated from the roof. The mixing efficiency of the flow is predicted to be about 0.9 over the complete range in height H . Therefore we expect that the mixing of descending thermal plumes was extensive over most of the time it took for the floor to meet the roof of the lava lake. However, from examination of the experimentally-determined concentration profile for $E = 0.91$ in Fig. 2b we also expect that although the bulk of the lava lake should have been well-mixed by a large-scale convective circulation, minor thermal stratification may have been produced at the floor. One implication of this result is that although cooling at the roof will be distributed nearly uniformly by the flow, the amount of cooling influencing the lake at any time will be slightly less than if mixing was complete. A potentially more important implication is that the production of thermal stratification could enhance cooling, and hence crystallization, at the floor.

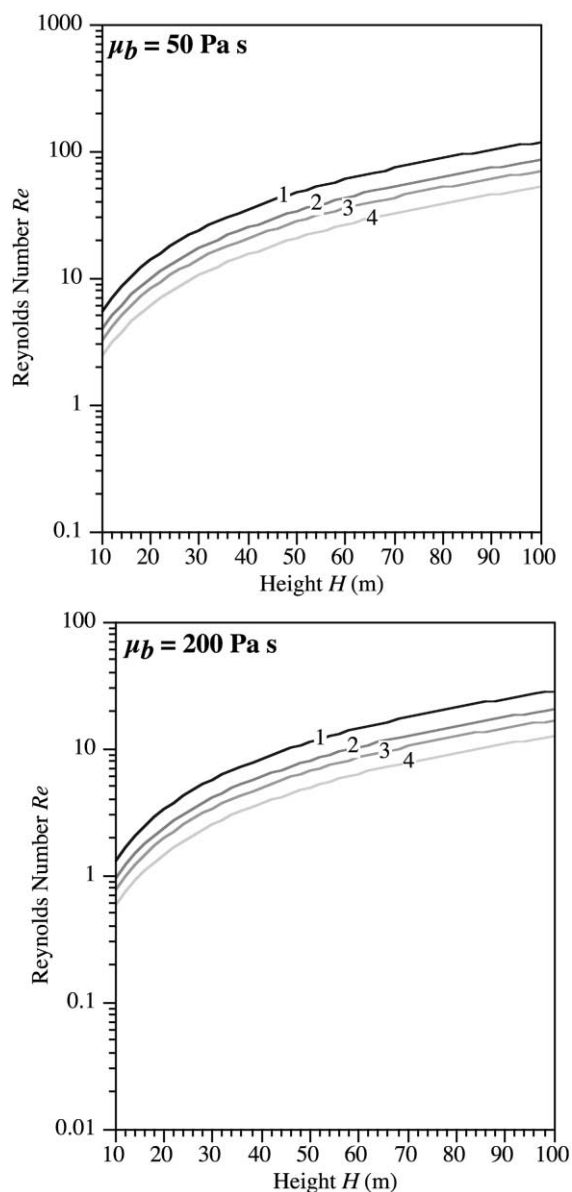


Fig. 4. Plots of the Reynolds number Re as a function of height H for the magma viscosities shown. The curves correspond to buoyancy fluxes due to: (1) crystal-rich thermal plumes descending from the roof, (2) crystal-free thermal plumes descending from the roof, (3) compositional plumes ascending from the floor, and (4) (latent heat) thermal plumes ascending from the floor.

3.2. Buoyancy fluxes due to cooling at the floor and sloping sidewalls

Heat flow from the magma to underlying floor

rocks combined with thermal convection driven by roof cooling is envisaged to have caused the magma at the floor to cool and crystallize. The in situ growth of olivine crystals at the floor will produce fluxes of buoyant residual liquid, and will form compositional boundary layers adjacent to olivine crystal/liquid interfaces (Martin et al., 1987). These gravitationally unstable boundary layers will detach and rise into the overlying magma where they become sufficiently thick that their buoyancy overcomes retarding viscous stresses and the dissipative effects of compositional diffusion (see also Seedhouse and Donaldson (1996). In the compositional boundary layer, the unstable density difference due to crystallization $\Delta\rho_c = (\rho_{fi} - \rho_b)$ is about 250 kg m^{-3} . A corresponding buoyancy flux per unit area of residual liquid is

$$B_c \sim V_c g \frac{\Delta\rho_c}{\rho_b}, \quad (11)$$

where the global conservation of heat requires the solidification rate

$$V_c \sim \frac{q_f}{\rho_b \left(L + c_b \frac{\partial T}{\partial S} \right)}. \quad (12)$$

Here, q_f is the heat flux at the floor and $\partial T/\partial S$ is the slope of the liquidus in temperature T –composition S space. The floor heat flux q_f depends on contributions from both the conductive heat loss to underlying floor rocks and from thermal convection driven by roof cooling. Whereas the heat flux to the floor (q_g) was estimated to be 100 W m^{-2} in Section 2, the proportion of roof cooling influencing the floor is more difficult to constrain. Although we have predicted thermal convection to be vigorous, because of the probably significant internal crystallization in the lake magma, it is uncertain how much of the roof cooling will reach the floor. Acknowledging the influence of thermal convection on cooling at the floor, we take the floor heat flux q_f to be 150 W m^{-2} . We note that because the Reynolds number will depend only on the one-third power of the floor heat flux q_f , the uncertainty over the influence of roof cooling is not significant. Substituting this heat flux and the appropriate values from Table 1 into Eqs. (12) and (11) gives a compositional buoyancy flux per unit area of $2.3 \times 10^{-8} \text{ m}^2 \text{ s}^{-3}$ (or alternatively a buoyancy force per unit area and time of $6.2 \times 10^{-5} \text{ N m}^{-2} \text{ s}^{-1}$).

The in situ growth of olivine crystals at the floor will also release latent heat, producing a thermal buoyancy flux per unit area

$$B_L \sim \frac{V_c g L \alpha}{c_b} \quad (13)$$

of $1.0 \times 10^{-8} \text{ m}^2 \text{ s}^{-3}$, where the density $\rho_b L \alpha / c_b$ is 86 kg m^{-3} . However, this unstable buoyancy flux is more than offset by the *stabilizing* buoyancy flux due to the heat flux to the floor ($B_t \sim q_g \alpha g / \rho_b c_b$) of order $1.4 \times 10^{-8} \text{ m}^2 \text{ s}^{-3}$, so that the net thermal buoyancy flux is stabilizing and of order $0.4 \times 10^{-8} \text{ m}^2 \text{ s}^{-3}$.

Since the compositional buoyancy flux is very much larger than the net thermal buoyancy flux, an appropriate Reynolds number for the convection from the floor can be based on the compositional buoyancy flux alone. Reynolds numbers based on the compositional buoyancy flux B_c are shown as a function of lake height H in Fig. 4 along with the Reynolds numbers determined previously for the roof thermal buoyancy fluxes. For an initial height $H = 100 \text{ m}$ and kinematic viscosities of 0.02 and $0.08 \text{ m}^2 \text{ s}^{-1}$, Reynolds numbers are 70 and 17, respectively. After the lake magma height H declines to 10 m, these Reynolds numbers become 3.2 and 0.8, respectively. Assuming for the present that crystallization takes place at the top of the floor solidification front in approximate thermodynamic equilibrium with the magma, there will be only a very small difference between the bulk compositions, and hence kinematic viscosities, of the residual liquid and the melt phase in the magma. The viscosity ratio then depends on whether ascending compositional plumes contain a volume fraction of crystals comparable to the magma. In one extreme, the compositional boundary layer is pure melt, which will have a kinematic viscosity of around $0.01 \text{ m}^2 \text{ s}^{-1}$. On the basis of the same range in magma viscosities, the viscosity ratio U lies between 2 and 8. In an alternative scenario compositional boundary layer fluid is rheologically similar to the magma and so $U \approx 1$. We note that it is difficult to imagine that this boundary layer fluid will be free of crystals, and so we suggest that a more realistic maximum viscosity ratio is probably 4. The Reynolds number Re –viscosity ratio U parameter space predicted for this compositional convection is shown in Fig. 2a. In addition, several photographs of experiments with compositional convection conducted

under a comparable range of $Re-U$ conditions are shown in Fig. 5 (see Jellinek et al. (1999) for a full discussion of these experiments). An average mixing efficiency E over most of the solidification history is between 0.7 and 0.9, and can be plausibly taken to be about 0.8. Inspection of Figs. 2b and 5 indicates that for this mixing efficiency, the magma will have a somewhat lower concentration over most of the lake than if mixing had been complete, as well as a modest compositional stratification at the roof.

In addition to fluxes of buoyant fluid from the top of the growing floor there is a possibility that buoyant residual liquid could be released into the overlying magma from within the floor zone as a consequence of compositional convection in the mush itself. The heat flow from the lava lake magma to the underlying floor and sidewalls will set up a temperature gradient in the floor crystal mush spanning the temperature interval between the liquidus and the solidus of the magma. As a consequence, residual liquid produced by the crystallization of intercumulus phases in the coldest lower part of the temperature gradient will be less dense than residual liquid produced in the hot upper part of the floor, resulting potentially in the convection of interstitial melt (Tait and Jaupart, 1992, 1996; Worster, 1992, 1997). The main factors controlling mush convection in the floor are the driving density difference $\Delta\rho_m$, the permeability χ , height h_f , and thermal diffusivity κ_m of the floor mush, and the kinematic viscosity of the mush fluid ν_m . For the physical properties of the floor cumulate given in Table 1, the thickness at which significant convection will occur in the floor

$$h_f^c = \frac{25 \kappa_m \rho_m \nu_m}{g \Delta\rho_m \chi} \quad (14)$$

(cf. Tait and Jaupart, 1992) is about 10 m, or after roughly one sixth of the floor zone was formed.

The results from the experiments of Tait and Jaupart (1992) show that a plausible consequence of convection through mush is the formation of axisymmetric chimneys through which buoyant interstitial melt can drain from deep within the mush into the overlying magma. Chimneys have diameters and spacings significantly greater than the spacing between compositional plumes ascending from the compositional boundary layer at the top of the floor solidification front. These structures form because

upwelling interstitial melt that is in thermodynamic equilibrium with the cold part of the temperature gradient in the floor becomes undersaturated as it ascends into the higher temperature upper part of the floor, resulting in the dissolution of cumulus crystals and, in turn, the formation of axisymmetric pathways. We note that the corresponding returnflow of magma into the floor will become supersaturated as it descends down the temperature gradient in the floor, leading to further growth of cumulus crystals and a reduction in porosity.

The axisymmetric structure, evolved bulk composition, relatively broad spacing (greater than the diameter of a single drill core), and the appearance of VORBS in the upper one third of the floor zone suggests the possibility that these highly-differentiated bodies are fossil chimneys. Helz (1980, 1987a) has suggested that because VORBS and segregation veins have similar interstitial compositions, that they are related to one another. As segregation veins were produced continually over the solidification history of the lake (Helz, 1980), for this hypothesis to be correct fluid released from chimneys must have been mixed negligibly by the vigorous motions expected to occur in the magma. Unfortunately, the mixing of a VORB-like fluid released from a chimney is difficult to evaluate because the influence of ambient convective motions is currently unknown (cf. Huppert et al., 1986). In addition, VORB magmas appear to have had a large but uncertain concentration of $H_2O_{(v)}$ bubbles that could have affected both the buoyancy and rheology of these compositional plumes (see also Goff, 1996).

One test of the validity of the hypothesis that VORBS are fossil chimneys is a comparison of the total volume of segregation vein material in the roof with the volume of buoyant fluid released from a single chimney over the time it took for the floor zone to meet the roof zone. Assuming that segregation veins occupy about 10 vol% of the roof (Helz, 1980, 1987a), the volume of segregation vein material in the roof is around $2 \times 10^6 \text{ m}^3$. Taking the flow rate through a given VORB chimney

$$Q = \frac{\pi g \Delta\rho_m d^4}{128 \rho_b \nu_m} \quad (15)$$

(Tritton, 1988), where the diameter $d \approx 5 \text{ cm}$, the

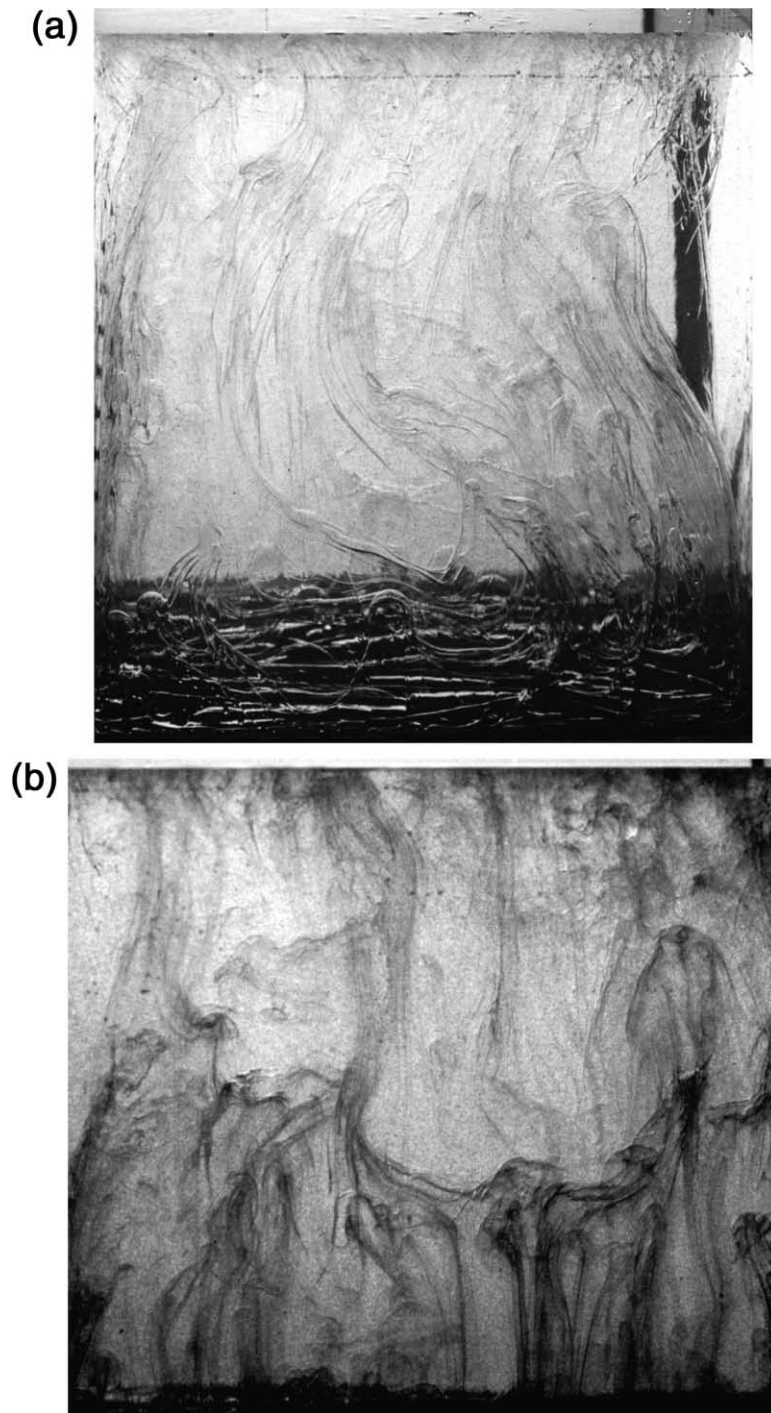


Fig. 5. Photographs of experiments with compositional convection conducted under dynamical conditions appropriate to the 1959 Kilauea Iki lava lake. The stirring associated with these complex, highly unsteady flows has produced minor compositional stratification, which is indicated by the dark fluid ponded at the top of each photograph. (a) $Re = 1$ and $U = 11$. (b) $Re = 7$ and $U = 1.7$.

total volume of magma ascending through a chimney over a time t of 10 yr, say, is about 10^3 m^3 . As this volume is much less than the total volume of segregation vein material in the roof, it is plausible that segregation veins were produced by a flux of evolved magma from about two thousand chimneys distributed over the floor.

Another important source of buoyancy we have not yet considered is the ascent of gas bubbles either exsolved from the magma as a result of crystallization or inputted from the floor as a consequence of the circulation and boiling of groundwater and hydrothermal fluids. Indeed, on the basis of a preliminary analysis of the concentrations of H_2O in samples of drill core Helz et al. (1989b) have asserted that 'clearly H_2O was being added to the lake'. At present, however, there are constraints on neither the total input of meteoric water into the magma, nor the geometry, spacing, and lifetime of potential sources. An additional uncertainty arising due to the potential for a free slip boundary condition at the interface between a bubble and surrounding magma is the extent to which ascending bubbles transmit momentum to the magma, and hence drive convection. As a result, we cannot yet assess the flow resulting from the input of $\text{H}_2\text{O}_{(v)}$ bubbles from the floor hydrothermal system. Turning to the bubbles released from the magma, understanding the resulting convection requires constraints on the total flux of gas, the size and composition of the bubbles, where the exsolution is predominantly occurring and a time scale for the process. Owing to the low hydrostatic pressure and low concentrations of principally S and CO_2 in the lake, the predominant volatile phase exsolved in compositional boundary layers was probably $\text{H}_2\text{O}_{(v)}$ (Harris and Anderson, 1983; Gerlach and Graeber, 1985; Gerlach, 1986). Initially, the exsolution of dissolved $\text{H}_2\text{O}_{(v)}$ would have occurred throughout the lake, predominantly at the margins of crystals growing at the roof and floor solidification fronts as well as internally. However, the solubility of H_2O is predicted to decline significantly with the drop in pressure over the small height of the lake magma (Gerlach, 1986). Therefore, for a given concentration of H_2O in the magma, there will be a bias of bubble exsolution towards the top of the lake. As a consequence, because overturning motions in the lake will continuously advect magma from the floor to the roof, where

$\text{H}_2\text{O}_{(v)}$ will be increasingly exsolved, the concentration of H_2O in the magma will become ultimately set by the low solubility of H_2O at the roof (Woods and Cardoso, 1997; Cardoso and Woods, 1999). Over time, then, a bubble gradient could develop with the magma nearest the floor becoming increasingly undersaturated with respect to H_2O , a feature that could inhibit thermal convection from the roof (Davaille and Jaupart, 1993b; Worster et al., 1993). The timescale for this process to occur is given by the lava lake depth divided by the Stokes rise velocity of the bubbles. For dynamic viscosities μ_b of 50–200 Pa s and for the bubble diameters of 1–10 mm found in the upper 10 m of the roof (Richter and Moore, 1966), this timescale is less than a few months.

To this point we have ignored the influence of the sloping sidewalls on the convection and mixing, treating the lava lake as essentially a sheet-like body. However, experiments with convection from sloping boundaries (Martin and Campbell, 1988) have shown that buoyant residual liquid will initially ascend towards the top of the lake as a gravity current for only about one boundary layer thickness before becoming unstable, detaching, and ascending into the overlying magma as a field of highly unstable plumes. Hence, the sloping walls will have an insignificant influence on the compositional convection.

3.3. An average mixing efficiency for the convection in the lake

To determine the quantitative influence of thermal and compositional convection on the crystallization and chemical differentiation of the lake magma requires an assessment of an average mixing efficiency of the convective stirring. As the main thermal and compositional buoyancy fluxes are from opposing boundaries we can expect them to augment one another in a straightforward way. Because the Reynolds number depends on the one-third power of the total buoyancy flux, a Reynolds number based on the sum ($B_t^c + B_c$) is only a few percent larger than a Reynolds number based on the thermal buoyancy flux B_t^c alone. Hence, we take the Reynolds number based on B_t^c to be a good estimate of the Reynolds number for convection in the lava lake. Inspection of Fig. 2a

indicates that whereas the average mixing efficiency will remain 0.9 for thermal plumes descending from the roof, the average mixing efficiency for the stirring of compositional plumes ascending from the floor is around 0.8. We note that these mixing efficiencies will also probably be unaffected by the additional forcing due to ascending bubbles or crystal sedimentation. However, in addition to considering the mixing efficiency for the large-scale flow, it is important to consider the local interaction between ascending and descending plumes and stabilizing stratification. Descending thermal plumes will potentially drag and entrain magma forming the compositional stratification at the roof. Similarly, ascending compositional plumes will weaken thermal stratification at the floor. As these interactions will increase the effective mixing efficiency of the flow, a plausible mixing efficiency of the circulation for thermal and compositional plumes is 0.9. We note that this estimate may be conservative, depending on the extent to which the thermal and compositional stratification is destroyed.

Our prediction that convection produced extensive thermal and chemical mixing in the 1959 Kilauea Iki lava lake is largely consistent with the fluid dynamical modeling of Worster et al. (1993), in which it was assumed that thermal convection from the roof of a lava lake will produce complete mixing. The central difference to Worster et al. (1993) is that our average mixing efficiency $E = 0.9$ was determined in a forward way from an analysis of the convection in the lava lake formulated on the basis of the geological constraints on cooling and crystallization outlined in Section 2. Our approach is more closely tied to available geological data, and embodies a somewhat different dynamical picture to the study of Worster et al. (1993): (1) heat loss from the lava lake is significantly increased by hydrothermal penetration of the roof and floor; (2) the unstable thermal boundary layer at the roof is envisaged as containing abundant unconnected crystals that augment the buoyancy forcing driving thermal convection; (3) the floor is taken to have a cumulate porosity of 50–60 vol% rather than zero; (4) in the floor cumulate, there was probably mush convection that may have led to chimney formation; (5) compositional and potentially bubble convection (including the possible release of VORB magmas from chimneys) from the floor augmented motions driven by thermal

convection from the roof; and (6) the convection may have led to minor thermal and compositional stratification.

4. Chemical differentiation of the lava lake

From the results of the analysis in Section 3 we can infer that one of the primary processes leading to the chemical differentiation of the 1959 Kilauea Iki lava lake was the extensive but imperfect convective mixing of residual liquid released to the magma as a consequence of crystallization at the roof and floor solidification fronts, and internally. The main influence on differentiation of the production of minor compositional stratification is that there is a net flux of residual liquid, and hence incompatible components, from the floor to the roof. At the roof, residual liquid produced during the growth of olivine crystals suspended in the thermal boundary layer could be carried into the underlying magma by descending, crystal laden, thermal plumes. Whereas ambient vigorous motions would disperse most of the entrained crystals, residual liquid would become mixed into the magma. Conversely, at the floor the flux of buoyant residual liquid from the top of the solidification front will augment convective circulation due mostly to roof cooling, leading, in turn, to its becoming mixed. Residual liquid ascending from thin compositional boundary layers around crystals growing internally is expected to be mixed completely. A second important differentiation mechanism leading to a net flux of magma from the floor to the roof was identified to be the rise of highly evolved VORB magmas from axisymmetric chimneys or pipes in the floor zone, which Helz (1980) has suggested may have led to the production of the segregation veins that comprise around 10 vol% of the roof. In addition to the convection discussed in Section 3, we note that some other postcumulus processes that could potentially lead to a flux of evolved magma from the floor to the roof are the compaction (cf. Philpotts et al., 1996) and cracking of the floor zone. Whereas there is no clear petrographic evidence of significant compaction in the floor (see Section 2) whether cracking was important cannot be resolved from the drill core available.

To evaluate the significance of the predicted

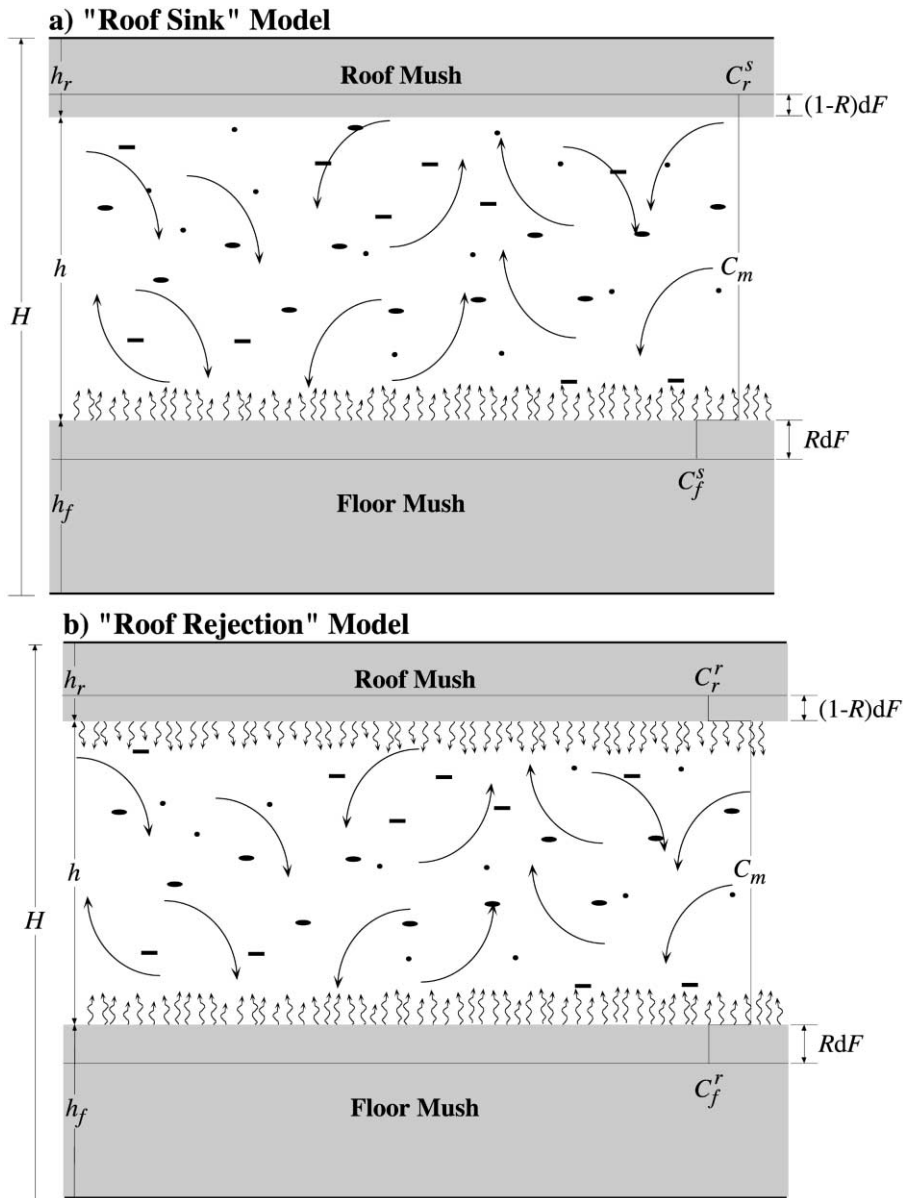


Fig. 6. Definition sketches for the (a) 'roof sink' and (b) 'roof rejection' models.

extensive mixing of residual released from the roof and floor solidification fronts and from olivine crystals growing internally, we develop two geochemical models based on the well-understood principles of Rayleigh fractionation. That is, chemical differentiation of the magma is a consequence of the separation of crystals from the melt phase in the magma. In

the first 'roof sink' model, differentiation occurs because of a combination of the convective mixing of buoyant residual liquid ascending from crystals growing in situ at the floor, and the mixing of residual liquid left behind by crystals settling from the interior magma. Due to its stabilizing buoyancy, residual liquid produced at the roof solidification front remains

Table 2
Parameters used in chemical modeling

Parameter	Symbol	Value and/ or unit
Constants	A, B	–
Concentration*	C	–
Distribution coefficient	D	–
Enrichment factor	ϵ	–
Fraction of lava lake remaining	F	–
Fraction of liquid remaining in an arbitrary volume of magma	F_V	–
Height of the magma	h	m
Height of the floor	h_f	m
Height of the roof	h_r	M
Constant	K	0.1
Ratio of the floor height to the total height crystallized at the roof and the floor	R	–
Dimensionless height	Z	–
Compositional difference across the compositional boundary layer	ΔS	–
Compositional expansion coefficient	β	7×10^{-2}
Compositional boundary layer thickness	δ_s	m
Mush porosity	ϕ	–
Weighting parameters	γ, θ	–
Subscripts on the concentration C	Meaning:	
c	Residual liquid	
f	Floor	
fm	Floor melt	
0	Initial	
m	Melt	
r	Roof	
rm	Roof melt	
s	Solid	
Superscripts on the concentration C	Meaning:	
r	Roof rejection model when the mixing efficiency $E = 1$.	
s	Roof sink model when the mixing efficiency $E = 1$.	
s*	Roof sink model when $E \leq 1$.	

* Concentrations are listed as dimensionless because they are normalized to an initial bulk composition. Hence, $C_0 = 1$.

there, and cannot influence the chemical evolution of the underlying magma. In an alternative ‘roof rejection’ model, residual liquid produced at the roof solidification front is envisaged to be also stirred into the magma as a consequence of being entrained in descending thermal plumes. An initial assumption made in formulating both models is that mixing is complete (the mixing efficiency $E = 1$). After comparison of these initial results with chemical data recorded in Fig. 3, we relax the constraint of complete convective mixing and explore the additional influence on differentiation of the production of minor compositional stratification at the roof. Further refine-

ment of our understanding of the chemical data is obtained with considerations of the additional effect of mush convection in the floor and roof zones.

4.1. Rayleigh fractionation models assuming complete mixing ($E = 1$)

The two fractionation models are outlined schematically in Fig. 6 and the parameters used in the modeling are defined in Table 2. We take the lava lake to have an initial height H and an initial bulk composition C_0 . Solidification progresses through in situ olivine crystallization at the floor and roof, and

through the sedimentation of crystals nucleated internally which, in turn causes the height of the magma h to decline. The roof and floor zones are taken to be mushes composed of a volume fraction ϕ of interstitial melt with concentration C_m and a volume fraction $(1 - \phi)$ of olivine crystals, each with a trace element concentration $C_s = C_m D$, where D is an equilibrium distribution coefficient (and $D \ll 1$ for highly incompatible trace elements). It was established in Section 2 that the height of the floor zone h_f is significantly greater than the height of the roof zone h_r , implying that the floor grew faster than the roof. Accordingly taking $F = h/H$ to be the fraction of lava lake remaining at any time, we define the ratio $R = h_f/(h_f + h_r)$ such that the respective growths of the floor zone $h_f/H = R(1 - F)$ and the roof zone $h_r/H = (1 - R)(1 - F)$.

In the roof sink model (Fig. 6a), residual liquid is retained within pores separating cumulus olivine crystals in the roof, and so at each increment of fractionation $(1 - R)dF$ the roof solidification front will have a bulk composition that is identical to the bulk composition of the underlying magma. Said differently, this approximation is equivalent to defining an effective distribution coefficient $D = 1$ in the roof only, such that $C_s = C_m$. Therefore, the bulk composition of the roof solidification front is

$$C_r^s = C_m \quad (16)$$

where the superscript 's' indicates 'roof sink' and the subscript 'r' indicates 'roof'. At the floor, where buoyant residual liquid is continually rejected into the overlying magma and mixed completely, the effective distribution coefficient is the equilibrium distribution coefficient, D , and so the bulk composition of the floor solidification front at each increment of fractionation RdF is

$$C_f^s = [\phi + (1 - \phi)D]C_m, \quad (17)$$

where the subscript 'f' indicates 'floor'. The governing equation for the change in concentration of an incompatible element in the magma with olivine fractionation is

$$\frac{dC_m}{dF} = \frac{C_m}{F} (\phi + [(1 - \phi)D - 1]R), \quad (18a)$$

which with the initial condition

$$C_m = C_0 \quad \text{when } F = 1 \quad (18b)$$

can be integrated to obtain

$$C_m^s = C_0 F^{(\phi + ((1 - \phi)D - 1)R)}. \quad (19)$$

Turning to the 'roof rejection' model (Fig. 6b), thermal convection from the roof stirs residual liquid from the roof solidification front into the underlying magma. Therefore, as for the floor solidification front, the effective distribution coefficient at the roof is the equilibrium distribution coefficient, D . Modifying Eq. (16), at each increment of fractionation $(1 - R)dF$ the bulk composition of the roof solidification front becomes

$$C_r^r = [\phi + (1 - \phi)D]C_m, \quad (20)$$

where the superscript 'r' indicates 'roof rejection'. As the expression for the bulk composition of the floor zone remains given by Eq. (17), the governing equation for the change in incompatible element concentration in the magma with fractionation is

$$\frac{dC_m}{dF} = \frac{C_m}{F} (D - 1)(1 - \phi), \quad (21)$$

which with Eq. (18b) is integrated to give

$$C_m^r = C_0 F^{(D-1)(1-\phi)}. \quad (22)$$

We note that Eq. (22) is identical to the fractionation equation obtained by Campbell (1987) in a study of the differentiation of the Jimberlana mafic layered intrusion in which $R = 1$. For cases in which $R \neq 1$, the roof rejection model is consistent modeling of Shirley (1987) for the Palisades sill. In addition, for the special case of $R = 1$ and $\phi = 0$, both Eqs. (19) and (22) are reduced to the classical equation for perfect Rayleigh fractionation $C_m = C_0 F^{(D-1)}$.

Concentration profiles predicted with Eqs. (19) and (22) are shown in Fig. 7 along with normalized bulk chemical data for the incompatible elements K_2O and TiO_2 from samples of drill core covering the upper 90 m of the lake height. The dimensionless height $Z = z/H$ and from examination of Fig. 3 the ratio R is taken to be 0.58. The melt compositions predicted by the two models have been corrected to bulk compositions by multiplying them by the liquid fraction ϕ (because $D = 0$ for incompatible elements). We have taken

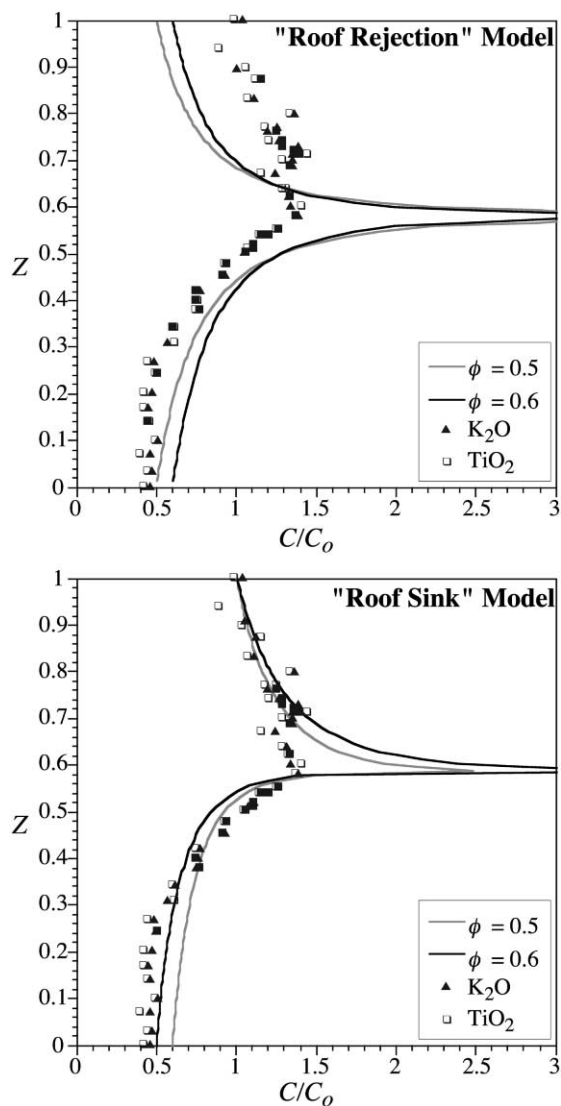


Fig. 7. Plots of normalized concentration profiles predicted with Eqs. (19) and (22) using the range of cumulate porosities identified in Section 2. See text for discussion.

the interstitial melt fraction to be in the range $0.5 \leq \phi \leq 0.6$, in accordance with the petrological constraints outlined in Section 2. Comparison of the fields separating the $\phi = 0.5$ and 0.6 profiles with the incompatible element data indicates that although neither model is excellent, the 'roof sink' model better captures the variation in the incompatible element data averaged over the height of the lake shown.

The main difference between the results of the two models is that whereas the quality of the fits over the depth of the floor is comparable, the 'roof sink' model better captures the chemical variation in the roof, implying that the roof contributed little residual liquid to the underlying magma over the course of solidification. Although potentially explained in part by uncertainties over the porosity ϕ , notably consistent shortcomings in both models are over-predicted enrichments over the lower half of the floor and between $Z = R$ and $Z \approx 0.66$. In addition, the roof sink model underestimates the data by 10 or 15% between $Z \approx 0.4$ and $Z = R$.

4.2. A 'roof sink' fractionation model for arbitrary mixing efficiencies ($E \leq 1$)

From the analysis presented in Section 3, modeling assuming a mixing efficiency $E = 1$ is applicable strictly only if the growth of the floor is controlled by the sedimentation of crystals nucleated internally. This is the case because we expect complete mixing of the thin boundary layers of residual liquid released from the margins of the crystals. However, it was also argued in Section 3 that the large cooling at the floor would have led to significant in situ olivine crystallization resulting, in turn, in the release of buoyant residual liquid that would be mixed extensively but incompletely (average mixing efficiency $E = 0.9$). Accordingly, we explore whether the influence of imperfect mixing can resolve some of the discrepancy between the chemical data and the roof sink models discussed above. Inspection of Fig. 2b indicates that the main effect of the convection will be to enrich modestly the magma at the roof in buoyant residual liquid, and hence incompatible elements. However, an important difference to our experiments is that the diffuse crystal mush forming the solidification front at the roof of the lava lake was a highly permeable boundary. A significant implication of this boundary condition is that buoyant fluid predicted to pond at the roof on the basis of our results could ascend further into the roof, displacing less buoyant interstitial melt more depleted in incompatible elements downward. Therefore, it is unclear whether all or part of the steep concentration gradient suggested by the $E = 0.91$ profile in Fig. 2b will affect crystallization at the roof solidification front.

Although the experimental results cannot be used to make quantitative predictions about the concentration of residual liquid from the floor in the magma involved in roof crystallization, we can use them as a guide and investigate the effects of a plausible range of residual liquid concentrations in magmas at the roof and floor. Incorporating the influence of additional residual liquid from the floor solidification front in the melt in contact with the crystals forming the roof solidification front, the new concentration in the melt phase at the roof is

$$C_{rm} = C_m + \theta C_c. \quad (23)$$

Including the influence of residual liquid lost from the magma in contact with the floor to the magma at the roof, the new concentration in the melt at the floor is

$$C_{fm} = C_m - \gamma C_c, \quad (24)$$

where C_c is the concentration of incompatible components in the residual liquid resulting from in situ olivine crystallization at the floor, and θ and γ are weighting parameters with values between 0 and 1, which are discussed below.

The concentration of incompatible elements in the residual liquid depends on the dynamics controlling olivine crystallization. During olivine crystallization, the intermittent growth and detachment of thin compositional boundary layers drive compositional convection from the crystal–liquid interface. Assuming that K_2O and TiO_2 are perfectly incompatible in olivine, the extent to which these components are enriched depends on the amount of solid grown over the lifetime of a compositional boundary layer. The growth of olivine crystals over the time it takes a compositional boundary layer to become unstable and drain is controlled by the solute flux across the boundary layer, which is proportional to the attendant compositional gradient and inversely proportional to its thickness. The study of Martin et al. (1987) has shown that the boundary layer thickness

$$\delta_s \sim \left(\frac{\rho_b \nu_b \kappa_s^2}{K^3 g \beta V_c} \right)^{1/4} \quad (25)$$

and the compositional difference ΔS (expressed in

weight fraction)

$$\Delta S \sim \left(\frac{\nu_b}{g \beta \kappa_s^2} \right)^{1/4} (K V_c)^{3/4} \quad (26)$$

across a critically unstable compositional boundary layer depends mostly on the crystallization rate V_c (see Eq. (12)), and hence the heat flux q_f . Here, β is a compositional expansion coefficient and the constant $K = 0.1$. From examination of Eqs. (12), (25), and (26) it is clear that the boundary layer thickness δ_s and the compositional contrast ΔS will decrease and increase, respectively, as the cooling rate q_f becomes large. Applying relevant physical properties from Tables 1 and 2 and a conservative (but still very large) heat flux $q_f = 100 \text{ W m}^{-2}$ at the floor of the lava lake to Eqs. (25) and (26), we obtain a compositional boundary layer thickness of order 1 mm and a corresponding compositional difference of order 1.

This critical compositional difference implies that enough solid olivine must grow such that an unstable density difference to the overlying magma $\beta \Delta S$ of around 7% is achieved in the boundary layer. Applying this constraint to an arbitrary fixed volume of Kilauea Iki magma, we can estimate the fraction of liquid remaining F_V after this critical volume fraction of olivine has grown and, in turn, the resultant enrichment of a perfectly incompatible element in the liquid. From an expression for the density of this arbitrary volume of magma

$$\rho_b = F_V(\rho_b - \rho_b \beta \Delta S) + (1 - F_V)\rho_{fr}, \quad (27)$$

we obtain the liquid fraction corresponding to the critical solid fraction

$$F_V = \frac{1}{1 + \beta \Delta S \left(\frac{\rho_b}{\rho_{fr} - \rho_b} \right)}. \quad (28)$$

The resultant enrichment of a perfectly incompatible component ϵ in the liquid phase is then

$$\epsilon = \frac{1}{F_V}, \quad (29)$$

indicating a residual liquid concentration

$$C_c = \epsilon C_m. \quad (30)$$

Combining Eqs. (16), (23), and (30) leads to the bulk composition of the roof zone at each increment

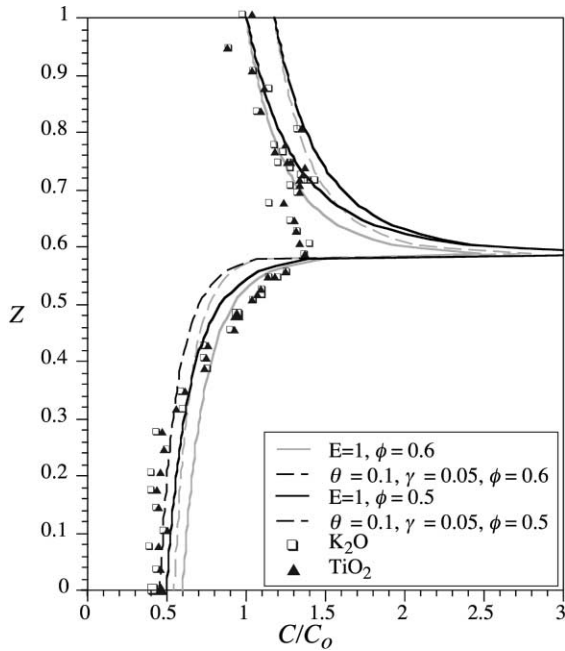


Fig. 8. A comparison of concentration profiles predicted with Eqs. (34a) (dashed line) and (19) (solid line). Curves for two porosities are shown to illustrate the overlap between the influences of imperfect mixing and uncertainties over the porosity ϕ .

of fractionation $(1 - R)dF$

$$C_r^{s*} = (\theta\epsilon + 1)C_m, \quad (31)$$

where ‘*’ is used to distinguish the ‘roof sink’ model developed for arbitrary mixing efficiencies E from the purely $E = 1$ case. Combining Eqs. (17), (24), and (30) gives the bulk composition of the floor zone at each increment of fractionation RdF

$$C_f^{s*} = (\phi + (1 - \phi)D)(1 - \gamma\epsilon)C_m. \quad (32)$$

The governing equation for the change in the concentration in the magma C_m^{rs*} with fractionation F becomes

$$\frac{dC_m^{s*}}{dF} = \frac{C_m}{F}(AR + B(1 - R) - 1), \quad (33)$$

which with Eq. (18b) is integrated to give

$$C_m^{s*}(F) = C_0 F^{AR + B(1 - R) - 1}, \quad (34a)$$

where the constants

$$A = (\phi + (1 - \phi)D)(1 - \gamma\epsilon) \quad (34b)$$

and

$$B = \theta\epsilon + 1. \quad (34c)$$

We note that when mixing is complete, Eq. (34) reduces to Eq. (19).

Applying a typical Kilauea Iki olivine fractionation density $\rho_{fr} \approx 2950 \text{ kg m}^{-3}$ with values for ρ_b and β contained in Tables 1 and 2 to Eqs. (28) and (29) indicates that residual liquid produced at the floor will be enriched in incompatible elements relative to the main magma by about a factor $\epsilon = 1.75$, implying through Eq. (30) that the concentration $C_c = 1.75C_m$. In Fig. 8, concentration profiles calculated with Eq. (33) are shown for porosities ϕ of 0.5 and 0.6, a roof enrichment factor θ corresponding to a 10% addition of residual liquid to the magma at the roof ($\theta = 0.1$), and a floor depletion factor γ corresponding to a 5% loss of residual liquid from the magma floor ($\gamma = 0.05$). To illustrate the effect of imperfect mixing on differentiation, for two porosities, profiles calculated with Eqs. (19) and (33) are shown, forming fields. As expected, the main influence of incomplete mixing is to deplete the floor and enrich the roof in incompatible elements, resulting in a steepening of the concentration profiles. However, because there is a large overlap between the fields implied by each set of curves, whether the understanding of the chemical data is improved with consideration of incomplete mixing is unclear. Although the inclusion of the effect of minor compositional stratification may improve the fit to the data over the lower half of the floor and the roof we cannot separate the influence of incomplete mixing from the influence of the uncertainty about the porosity ϕ on differentiation. However, despite the difficulty in distinguishing the two effects, the data remain overestimated over the lower half of the floor and between $Z = R$ and $Z \approx 0.7$, and are under-predicted between $Z \approx 0.4$ and $Z = R$.

4.3. Mush convection in the roof and floor

Over the course of cumulus crystallization in the lava lake, residual liquid produced at the floor and roof solidification fronts became increasingly buoyant (due to the increasing iron content of the olivine (cf. Sparks and Huppert, 1984)) as well as enriched in incompatible elements. Therefore, one explanation for the overestimated enrichment in the roof as well

as the scatter in the chemical data is that the data record the influence of the convection, or continual 'leakage', of buoyant enriched magmas from the roof solidification front into the overlying highly-permeable crystal mush. The resulting circulation would act to homogenize existing compositional gradients, which is consistent with the roughly uniform chemical data between $Z = R$ and $Z \approx 0.7$ in Fig. 8.

In Section 3.2 it was predicted that the convection of interstitial melt could occur once the floor grew to about 10 m thick. We have hypothesized that this flow may have led to the formation of chimneys through which highly-evolved VORB fluids rose from within the floor mush into the overlying magma. VORB magmas ascending from chimneys will produce a net upward flux of incompatible elements from the lower part of the floor. In the absence of any significant compaction of the floor (cf. Section 2) an upflow of VORB fluids must be balanced by a downflow of magma into the underlying floor. In addition to enriching the roof, this circulation will affect the incompatible element concentration in the floor. However, the influence of this circulation on the vertical distribution of incompatible elements in the lake depends on the extent to which ascending highly-enriched VORB magmas are mixed by convective motions in the magma, which is currently unclear. In one extreme, buoyant VORB fluids are mixed completely and the magma overlying the floor becomes potentially strongly enriched in incompatible elements. In this situation, both interstitial melt at the roof solidification front and melt that flows into the floor will have a higher concentration of incompatible elements, leading to a net enrichment of the roof and upper floor. In another extreme, the mixing of these evolved fluids is negligible and they pass through the magma and pond at the roof solidification front or higher in the roof zone to help form segregation veins. Whereas the roof could become greatly enriched in incompatible elements, downflows of magma into the floor will have a comparatively lower incompatible element concentration. However, as the magma overlying the floor is continually enriched in incompatible elements during the growth of the floor, downflows will still enrich the floor in incompatible elements, but to a lesser extent than in the case of the complete mixing of VORB magmas.

To conclude, circulation resulting from mush

convection in the floor and roof is envisaged to have led to a depletion and an enrichment of incompatible elements in the lower half of the floor and in the upper half of the floor, respectively, as well as to the fairly homogeneous overpredicted incompatible element concentration in the lower half of the roof.

4.4. A comparison with previous work on Kilauea Iki and directions for future study

A central conclusion from our analysis of the differentiation of the lava lake is that most of the chemical variation can be explained as a consequence of a combination of crystal settling and the extensive but imperfect convective mixing of buoyant residual liquid released from the floor. A more complete understanding of the chemical variation over the height of the lake requires a net flux of incompatible elements to the upper third of the floor zone and to the roof. We have argued that this flux can be explained as a consequence of a combination of the production of minor compositional stratification by convection in the lake magma and mush convection in the roof and floor zones. The importance of a net transfer of incompatible components to the upper part of the floor and to the roof was first recognized by Helz et al. (1989a), who argued that a large volume of residual liquid had been extracted from the interval $0.14 \leq Z \leq 0.38$ and deposited over the interval $0.66 \leq Z \leq 0.86$ between 1960 and 1971. However, in contrast to the physical picture we have constructed, these authors envisaged a continuous process in which plumes of low density interstitial melt rose from the floor, through a quiescent magma, and into the roof without mixing. Given the geological constraints on the cooling, composition, and physical properties of the magma identified in Section 2 and the buoyancy sources discussed in Section 3, it is unclear how the lake magma could have remained quiescent over much of its solidification history.

In the chemical modeling presented in Sections 4.1–4.3 we have restricted our attention to the effects of convection and crystallization on the vertical distribution of nearly perfectly incompatible trace elements. We chose this approach because we have good field and petrographical constraints on olivine crystallinity (i.e. the predominant liquidus phase). In principle our models are easily extended to compatible trace elements and to major elements. Hence

there is a temptation to explore the covariation of compatible and incompatible components to address problems such as the subliquidus crystallization of interstitial phases and the influence of incomplete mixing on the liquid line of descent of the magma. However, before this analysis may be done properly several issues affecting the bulk composition of the main and interstitial magmas must be first addressed, and they are exciting directions for future studies of the 1959 Kilauea Iki lava lake. These include: (1) the challenge of identifying the independent influences of the mixing efficiency E and the porosity ϕ ; (2) the quantitative effect of transient leakage from the magma ahead of the roof solidification front into the overlying roof zone; (3) the mixing efficiency of VORB magmas released from chimneys in the floor; and (4) the quantitative influence of circulation in the roof and floor zones on intercumulus crystallization therein. To complement this future work, additional thorough petrographical and geochemical studies of the interstitial plagioclase, pyroxene, and glass phases are needed. Rigorous constraints on vertical and, where possible, lateral variations in interstitial mineralogy, mineral chemistry, and glass chemistry would be invaluable in testing models developed to understand the importance of mush convection in the roof and the floor to the chemical differentiation of the lake. We note that because cumulus olivine crystals forming the roof and floor of the lake probably reequilibrated very quickly during cooling (Helz, 1987b; Scowen et al., 1991), any information recorded in olivine grains about primary crystallization will have been lost. Finally, constraints on the initial porosity of the roof and floor along with some understanding of how this porosity varies vertically and laterally are of great interest (cf. Philpotts et al., 1998; Philpotts and Dickson, 2000). In addition to resolving the importance of incomplete convective mixing in the magma these data may be used to establish whether mush convection (or compaction) occurred in the floor, and hence whether the formation of axisymmetric chimneys could have led to the release of VORB magmas.

5. Influence of compositional convection on growth of the floor

In view of the very large cooling rate at the top of

the lava lake, one of the most intriguing features of the 1959 Kilauea Iki lava lake is that the floor zone is much thicker than the roof zone. As the pressure effect on the liquidus temperature in the lava lake will be very small over its height (the freezing temperature at the floor will be around 0.1°C hotter than at the roof (cf. Campbell, 1996)), the thick floor becomes even more curious. Although the settling of crystals from the roof thermal boundary layer and the sedimentation of crystals nucleated internally probably contributed significantly to the growth of the floor, the imperfect mixing of thermal plumes descending from the roof and compositional plumes ascending from the floor may have had a significant impact on in situ crystallization at the floor. Whereas thermal stratification will enhance cooling at the floor, the production of compositional stratification will cause magma at the roof to have a lower MgO concentration, and hence liquidus temperature, than the magma at the floor (Roeder and Emslie, 1970). As a result, for a given temperature in the magma the level of supersaturation at the floor will be higher than that at the roof, leading, in turn, to more rapid crystallization at the floor. Additional cooling due to the persistence of minor thermal stratification will enhance this effect. We note that minor ponding of residual liquid may have also influenced the bulk compositions of the magmas in contact with the roof and floor sufficiently such that plagioclase and pyroxene saturation was favored at the roof relative to the floor over the course of solidification. This could explain not only the greater presence of plagioclase and pyroxene phases in the roof zone, but also the observation that augite rims olivine crystals in the lower half of the roof zone (Helz, 1987b, p. 698).

To investigate the quantitative influence of incomplete mixing on the difference between the liquidus temperatures at the floor and roof in a way consistent with the analysis in the Section 4, we explore the effects of a 10% enrichment of residual liquid at the roof and a 5% depletion of residual liquid at the floor. For comparison, we include also considerations of 20% enrichments of residual liquid at the roof and 10% depletions at the floor. Assuming an initial bulk composition of 8.47 wt% MgO (cf. Section 2) and, for simplicity, pure olivine crystallization, the Roeder and Emslie (1970) relationship between Fe/Mg ratios in olivine and coexisting melt can be used to obtain rough estimates for the

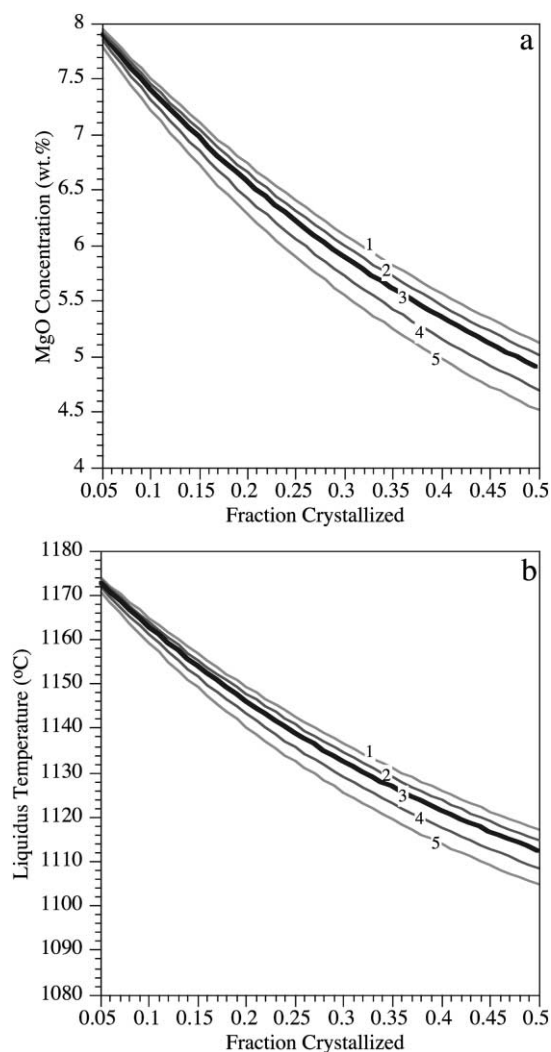


Fig. 9. Plots illustrating the influence of the incomplete mixing of residual liquid released from the floor solidification front on (a) MgO content and (b) liquidus temperature of the magma solidifying at the roof or the floor. The conditions are: (1) 20% enrichment, (2) 10% enrichment, (3) complete mixing ($E = 1$), (4) 5% depletion, and (5) 10% depletion.

concentration of MgO in the liquid as a function of the extent of olivine fractionation. Additional mass balance considerations can be applied to explore the effects of additional residual liquid at the roof and a depletion of residual liquid at the floor (Fig. 9a). Combining these predictions with the empirical MgO thermometer determined for the 1959 Kilauea Iki magma by Helz and Thornber (1987) leads, in

turn, to corresponding estimates of the liquidus temperatures at the roof and floor (Fig. 7b). We note that although plagioclase and augite joined the liquidus at around 1165°C (Helz and Thornber, 1987), the linear dependence of liquidus temperature on MgO concentration reported by Helz and Thornber (1987) is similar to that predicted using the method of Roeder and Emslie (1970) for pure olivine crystallization.

An initial MgO concentration of 8.47 wt% implies a liquidus temperature of 1184°C, which is in good agreement with the average emplacement temperature of 1185°C estimated by Ault et al. (1961). Examination of Fig. 9 indicates that after 20% crystallization, say, incomplete mixing producing a 10–20% enrichment in residual liquid at the roof solidification front will cause about a 0.15–0.30 wt% depletion in MgO relative to the case of complete mixing, implying a 2.5–5.0°C reduction in liquidus temperature. At the floor, a 5 to 10% depletion in residual liquid relative to the complete mixing case will cause the magma to be 0.08–0.16% enriched in MgO, which suggests a 1.3–2.6°C increase in liquidus temperature. Therefore, for the situation envisaged in Section 4.3 in which the magma crystallizing at the roof is 10% enriched in residual liquid while the magma crystallizing at the floor is 5% depleted in residual liquid, the liquidus temperature at the floor solidification front will be around 4°C higher than the liquidus temperature at the roof. In conclusion, a combination of the freezing temperature being much higher at the floor of the lava lake than at the roof during solidification, minor thermal stratification at the floor, the substantial sedimentation of olivine crystals, and perhaps the minor foundering of roof crust indicates that a thick floor zone should not be surprising.

6. Conclusions

We have used geological controls on the cooling, composition, and physical properties of the magma along with constraints on the relative thicknesses and structures of the floor and roof zones to develop an understanding of the main physical processes at work during the solidification of the 1959 Kilauea

Iki lava lake. We have, in turn, applied this physical insight to the quantitative understanding of the chemical differentiation and crystallization of the magma. The following are the main conclusions that can be drawn from this study:

(1) Cooling at the roof of the lava lake was probably enhanced by the boiling of rainwater that progressively penetrated into the roof crust (see also Richter and Moore, 1966; Hardee, 1980). An estimate for the roof heat flux is about 300 W m^{-2} . We argue that the circulation and possibly boiling of groundwater and hydrothermal fluids augmented also the cooling at the floor, and suggest that a plausible estimate of the floor heat flux is 100 W m^{-2} . We note that this conclusion is consistent with the cooling in other Hawaiian lava lakes of similar size. For example, the upper and lower tiers of columnar joints observed in cliff exposures of the prehistoric Makaopuhi lava lake were of similar height (Moore and Evans, 1967), implying comparable cooling rates at the roof and floor.

(2) We suggest that the correspondence between the large increase in olivine crystallinity and the sharp reversal in the symmetrical incompatible and compatible element trends at about 40 m (Fig. 3) marks the boundary between the roof and floor zones. As the floor is substantially thicker than the roof we can conclude that it grew much more quickly. A plausible time scale for the roof to meet the floor is about 10 yr.

(3) Vigorous stirring in the magma driven predominantly by the descent of crystal-laden thermal plumes from the roof and compositional plumes from the floor is predicted to have been an inevitable consequence of strong cooling at the roof and the floor. Resultant large scale circulation is predicted to have produced extensive but imperfect mixing over most of the time it took for the floor to meet the roof (the average mixing efficiency $E \approx 0.9$), leading, in turn, to the production of minor thermal and compositional stratification at the floor and roof, respectively. It is expected that the widespread distribution of the large cooling at the roof led to the significant internal nucleation of olivine crystals, the settling of which augmented the growth of the floor. We note that the predicted average mixing efficiency $E = 0.9$ of the stirring would have been unchanged by additional forcing due either to crystal sedimentation or to the ascent of gas bubbles. A further remark is that this

dynamic picture of the lava lake strongly contrasts with the view of Helz (1980) that convection ‘either did not occur at all or was active only briefly’, and with the view of Helz et al. (1989a) that diapiric melt transfer occurred ‘without mixing’.

(4) Mush convection in the floor cumulate may have become significant by the time the floor grew to about 10 m thick. A potential consequence of this flow is the formation of axisymmetric chimneys through which evolved magma may have drained from deep within the floor into the overlying magma and possibly the roof. We suggest that the pipe-like, highly evolved VORBs observed in the floor zone may be fossil chimneys, and hence that mush convection may have led to a significant net upward flow of evolved magma from the floor to the overlying magma or roof. In terms of the effect on the chemical differentiation of the lake, the circulation driven by the upflow of VORB magmas is envisaged to have led to a depletion of incompatible elements in the lower half of the floor and an incompatible element enrichment in the upper half of the floor and the roof.

(5) In addition to mush convection in the floor, we expect buoyant residual liquid both produced at the roof solidification front and gained from the floor as a result of incomplete mixing to have percolated or ‘leaked’ into the overlying highly-permeable cumulate, displacing less buoyant interstitial melt downward. The main effect of this circulation on the chemical evolution of the lake is to both enrich the roof in incompatible elements and homogenize concentration gradients therein, which is consistent with the observed chemical variation in the roof.

(6) The results of our geochemical modeling indicate that most of the incompatible element variation over the height of the lake can be explained as a consequence of a combination of crystal settling and the extensive but imperfect convective mixing of buoyant residual liquid released from the floor solidification front. A more complete understanding of the chemical data, however, requires a net flux of incompatible elements from the lower part of the floor to the upper third of the floor zone and to the roof. We have argued that this flux can be explained as a consequence of a combination of the production of minor compositional stratification by convection in the lake magma, mush convection and the formation of chimneys in the floor, and circulation in the roof resulting

from a leakage of buoyant magma from the roof solidification front into the overlying crystal mush. However, we note that although we predict that stirring in the magma will lead to minor compositional stratification, we are unable to distinguish the quantitative effect of incomplete mixing from the influence of uncertainties over the porosity of the floor on the vertical distribution of incompatible elements in the lake. The requirement of an upward flux of incompatible elements is consistent with the findings of Helz et al. (1989a).

(7) Over the course of solidification, the minor ponding of residual liquid released from the floor would have caused the magma in contact with the roof to have a significantly lower MgO concentration, and hence liquidus temperature, than the magma in contact with the floor. Therefore, for a given temperature in the magma in situ olivine crystallization at the floor will be more rapid than in situ olivine crystallization at the roof. A combination of this effect, potentially enhanced by the additional cooling due to minor thermal stratification at the floor, and the substantial sedimentation of olivine crystals is envisaged to have caused the floor to grow much more rapidly than the roof.

Acknowledgements

We thank G. W. Bergantz, S. Blake and A. R. Philpotts for very helpful comments, and R. T. Helz for supplying us with the USGS Open File Report 94-684. AMJ was supported by an Overseas Postgraduate Research Fellowship, an ANU PhD scholarship, and the Miller Institute for Basic Research during the completion of this study. RCK was supported by an Australian Research Council Fellowship.

References

- Ault, W.U., Eaton, J.P., Richter, D.H., 1961. Lava temperatures in the 1959 Kilauea eruption and cooling lake. *Geol. Soc. Am. Bull.* 72, 791–794.
- Bottinga, Y., Weill, D.F., 1970. Density of liquid silicate systems calculated from partial molar volumes of oxide components. *Am. J. Sci.* 267, 1067–1082.
- Campbell, I.H., 1987. Distribution of orthocumulate textures in the Jimberlana intrusion. *J. Geol.* 95, 35–54.
- Campbell, I.H., 1996. Fluid dynamic processes in basaltic magma chambers. In: Cawthorn, R.G. (Ed.). *Layered Intrusions*. Elsevier, Amsterdam, pp. 45–76.
- Cardoso, S.S.S., Woods, A.W., 1999. On convection in a volatile-saturated magma. *Earth Planet. Sci. Lett.* 168, 301–310.
- Carrigan, C.R., 1987. The magmatic Rayleigh number and time dependent convection in cooling lava lakes. *Geophys. Res. Lett.* 14, 915–918.
- Chakraborty, S., 1995. Diffusion in silicate melts. *Structure, Dynamics and Properties of Silicate Melts*, Ribbe, P. (Ed.). *Rev. Mineral.* 32, 411–503.
- Davaille, A., Jaupart, C., 1993a. Transient high Rayleigh number thermal convection with large viscosity variations. *J. Fluid Mech.* 253, 141–166.
- Davaille, A., Jaupart, C., 1993b. Thermal convection in lava lakes. *Geophys. Res. Lett.* 20, 1827–1830.
- Gerlach, T.M., 1986. Exsolution of H₂O, CO₂, and S during eruptive episodes at Kilauea volcano, Hawaii. *J. Geophys. Res.* 91, 12177–12185.
- Gerlach, T.M., Graeber, E.J., 1985. Volatile budget of Kilauea volcano. *Nature* 313, 273–277.
- Goff, F., 1996. Vesicle cylinders in vapor-differentiated basalt flows. *J. Volcanol. Geotherm. Res.* 71, 167–185.
- Hardee, H.C., 1980. Solidification in Kilauea Iki lava lake. *J. Volcanol. Geotherm. Res.* 7, 211–223.
- Harris, D.M., Anderson, A.T., 1983. Concentrations, sources, and losses of H₂O, CO₂, and S in Kilauean basalt. *Geochim. Cosmochim. Acta* 47, 1139–1150.
- Helz, R.T., 1980. Crystallization history of Kilauea Iki lava lake as seen in drill core recovered in 1967–1979. *Bull. Volcanol.* 43, 675–701.
- Helz, R.T., 1987a. Differentiation behavior of the Kilauea Iki lava lake, Kilauea volcano, Hawaii: An overview of past, present, and future work. *Magmatic Processes: Physicochemical Principles*, Mysen, B.O. (Ed.). *Spec. Publ. Geochem. Soc.* 1, 241–258.
- Helz, R.T., 1987b. Character of olivines in lava of the 1959 eruption of Kilauea volcano and their bearing on eruption dynamics. *US Geol. Surv. Prof. Pap.* 1350, 691–722.
- Helz, R.T., Thornber, C.R., 1987. Geothermometry of the Kilauea Iki lava lake, Hawaii. *Bull. Volcanol.* 49, 651–668.
- Helz, R.T., Kirschenbaum, H., Marinenko, J.W., 1989a. Diapiric transfer of melt in Kilauea Iki lava lake, Hawaii: a quick, efficient process of igneous differentiation. *Geol. Soc. Am. Bull.* 101, 578–594.
- Helz, R.T., Kirschenbaum, H., Marinenko, J.W., 1989b. Whole-rock analyses of drill core from Kilauea Iki lava lake, Kilauea volcano, Hawaii. *US Geol. Surv. Open File Rep.* 94-684, 64pp.
- Hort, M., 1997. Cooling and crystallization in sheet-like magma bodies revisited. *J. Volcanol. Geotherm. Res.* 76, 297–317.
- Huppert, H.E., Sparks, R.S.J., 1988. The generation of granitic magmas by intrusion of basalt into continental crust. *J. Petrol.* 29, 599–624.
- Huppert, H.E., Turner, J.S., 1991. Comments on “On convective style and vigor in sheet-like magma chamber” by Bruce D. Marsh. *J. Petrol.* 32, 851–854.
- Huppert, H.E., Sparks, R.S.J., Whitehead, J.A., Hallworth, M.A.,

1986. Replenishment of magma chambers by light inputs. *J. Geophys. Res.* 91, 6113–6122.
- Jackson, D.B., Kauahikaua, J., 1990. The high level water table beneath Kilauea volcano, Hawaii. *Eos* 71, 1676.
- Jarvis, R.A., Woods, A.W., 1994. The nucleation, growth and settling of crystals from a turbulently convecting fluid. *J. Fluid Mech.* 273, 83–107.
- Jaupart, C., Tait, S.R., 1995. Dynamics of differentiation in magma reservoirs. *J. Geophys. Res.* 100, 17615–17636.
- Jellinek, A.M.J., Kerr, R.C., 1999. Mixing and compositional stratification produced by natural convection. Part 2. Applications to the differentiation of basaltic and silicic magma chambers, and komatiite lava flows. *J. Geophys. Res.* 104, 7202–7207.
- Jellinek, A.M.J., Kerr, R.C., Griffiths, R.W., 1999. Mixing and compositional stratification produced by natural convection. Part 1. The experiments, and their application to the Earth's core and mantle. *J. Geophys. Res.* 104, 7183–7201.
- Kerr, R.C., 1994. Melting driven by vigorous compositional convection. *J. Fluid Mech.* 280, 255–285.
- Kerr, R.C., 1995. Convective crystal dissolution. *Contrib. Mineral. Petrol.* 121, 237–246.
- Kerr, R.C., Woods, A.W., Worster, M.G., Huppert, H.E., 1989. Disequilibrium and macrosegregation during solidification of a binary melt. *Nature* 340, 357–362.
- Kerr, R.C., Woods, A.W., Worster, M.G., Huppert, H.E., 1990. Solidification of an alloy cooled from above. Part II. Nonequilibrium interfacial kinetics. *J. Fluid Mech.* 217, 331–348.
- Langmuir, C.H., 1989. Geochemical consequences of *in situ* crystallization. *Nature* 340, 199–205.
- Marsh, B.D., 1988. Crystal capture, sorting, and retention in convecting magma. *Geol. Soc. Am. Bull.* 110, 1720–1737.
- Martin, D., 1990. Crystal settling and *in situ* crystallization in aqueous solutions and magma chambers. *Earth Planet. Sci. Lett.* 96, 336–348.
- Martin, D., Campbell, I.H., 1988. Laboratory modeling of convection in magma chambers: crystallization against sloping floors. *J. Geophys. Res.* 93, 7974–7988.
- Martin, D., Nokes, R., 1988. Crystal settling in a vigorously convecting magma chamber. *Nature* 332, 534–536.
- Martin, D., Nokes, R., 1989. A fluid dynamical study of crystal settling in convecting magmas. *J. Petrol.* 30, 1471–1500.
- Martin, D., Griffiths, R.W., Campbell, I.H., 1987. Compositional and thermal convection in magma chambers. *Contrib. Mineral. Petrol.* 96, 465–475.
- McBirney, A.R., 1995. Mechanisms of differentiation in the Skaergaard intrusion. *J. Geol. Soc. Lond.* 152, 421–435.
- McBirney, A.R., Noyes, R.M., 1979. Crystallization and layering of the Skaergaard intrusion. *J. Petrol.* 20, 487–554.
- Moore, J.G., Evans, B.W., 1967. The role of olivine in the crystallization of the prehistoric Makaopuhi lava lake, Hawaii. *Contrib. Mineral. Petrol.* 15, 202–223.
- Murata, K.J., Richter, D.H., 1966. Chemistry of the lavas of the 1959–60 eruption of Kilauea volcano, Hawaii. *US Geol. Surv. Prof. Pap.* 537A, 25 pp.
- Nelson, S.A., Carmichael, I.S.E., 1979. Partial molar volumes of oxide components in silicate liquids. *Contrib. Mineral. Petrol.* 71, 117–124.
- Philpotts, A.R., Dickson, L.D., 2000. The formation of plagioclase chains during convective transfer in basaltic magma. *Nature* 406, 59–61.
- Philpotts, A.R., Carroll, M., Hill, J.M., 1996. Crystal-mush compaction and the origin of pegmatitic segregation sheets in a thick flood-basalt flow in the Mesozoic Hartford basin, Connecticut. *J. Petrol.* 37, 811–836.
- Philpotts, A.R., Shi, J., Brustman, C., 1998. Role of plagioclase crystal chains in the differentiation of partly crystallized basaltic magma. *Nature* 395, 343–346.
- Richter, D.H., Moore, J.G., 1966. Petrology of the Kilauea Iki lava lake, Hawaii. *US Geol. Surv. Prof. Pap.* 537B, 26 pp.
- Richter, D.H., Murata, K.J., 1966. Petrography of the lavas of the 1959–60 eruption of Kilauea volcano, Hawaii. *US Geol. Surv. Prof. Pap.* 537D, 12 pp.
- Richter, D.H., Eaton, J.P., Murata, K.J., Ault, W.U., Krivoy, H.L., 1966. Chronological narrative of the 1959–60 eruption of Kilauea volcano, Hawaii. *US Geol. Surv. Prof. Pap.* 537E, 73 pp.
- Roeder, P.L., Emslie, R.F., 1970. Olivine-liquid equilibrium. *Contrib. Mineral. Petrol.* 29, 275–289.
- Roscoe, R., 1953. Suspensions. In: Hermans, J.J. (Ed.). *Flow Properties of Disperse Systems*. North Holland Publishing Company, Amsterdam, pp. 1–38.
- Scowen, P.A.H., Roeder, P.L., Helz, R.T., 1991. Reequilibration of chromite within Kilauea Iki lava lake. *Contrib. Mineral. Petrol.* 107, 8–20.
- Seedhouse, J.K., Donaldson, C.H., 1996. Compositional convection caused by olivine crystallization in a synthetic basalt melt. *Mineral. Mag.* 60, 115–130.
- Shaw, H.R., 1969. Rheology of basalt in the melting range. *J. Petrol.* 10, 510–535.
- Shirley, D.N., 1987. Differentiation and compaction in the Palisades sill, New Jersey. *J. Petrol.* 28, 835–865.
- Sparks, R.S.J., Huppert, H.E., 1984. Density changes during the fractional crystallization of basaltic magmas: fluid dynamic implications. *Contrib. Mineral. Petrol.* 85, 300–309.
- Sparks, R.S.J., Huppert, H.E., Koyaguchi, T., Hallworth, M.A., 1993. Disequilibrium and macrosegregation during solidification of a binary melt. *Nature* 361, 246–248.
- Tait, S.R., Jaupart, C., 1992. Compositional convection in a reactive crystalline mush and melt differentiation. *J. Geophys. Res.* 97, 6735–6756.
- Tait, S.R., Jaupart, C., 1996. The production of chemically stratified and accumulate plutonic rocks. *Mineral. Mag.* 60, 99–114.
- Thomas, D.M., Walker, G.P.L., Trysdell, F., 1990. Structural and geochemical constraints on fluid circulation within the Kilauea east rift zone. *Eos* 71, 1676.
- Tritton, D.J., 1988. *Physical Fluid Dynamics*. Oxford University Press, Oxford, 519 pp.
- Turner, J.S., 1973. *Buoyancy Effects in Fluids*. Cambridge University Press, Cambridge, 366 pp.
- Turner, J.S., Campbell, I.H., 1986. Convection and mixing in magma chambers. *Earth Sci. Rev.* 23, 255–352.
- Woods, A.W., Cardoso, S.S.S., 1997. Triggering basaltic volcanic eruptions by bubble-melt separation. *Nature* 385, 518–520.

- Worster, M.G., 1992. Instabilities of the liquid and mushy regions during the solidification of alloys. *J. Fluid Mech.* 237, 649–669.
- Worster, M.G., 1997. Convection in mushy layers. *Ann. Rev. Fluid Mech.* 29, 91–122.
- Worster, M.G., Huppert, H.E., Sparks, R.S.J., 1991. Convection and crystallization in magma cooled from above. *Earth Planet. Sci. Lett.* 101, 78–89.
- Worster, M.G., Huppert, H.E., Sparks, R.S.J., 1993. The crystallization of lava lakes. *J. Geophys. Res.* 98, 15891–15901.
- Wright, T.L., Peck, D.L., Shaw, H.R., 1976. Kilauea lava lakes: Natural laboratories for the study of cooling, crystallization, and differentiation of basaltic magma. In: Sutton, S.H., Manghnani, M.H., Moberly, R. (Eds.), *The geophysics of the Pacific ocean basin and its margin*. *Geophys. Monogr.* 19, 375–390.